Engineering Journal

American Institute of Steel Construction

Second Quarter 2009 Volume 46, No. 2

www.aisc.org

ENGINEERING JOURNAL

AMERICAN INSTITUTE OF STEEL CONSTRUCTION

Dedicated to the development and improvement of steel construction, through the interchange of ideas, experiences and data.

ENGINEERING JOURNAL (ISSN 0013-8029) is published quarterly. Subscriptions: Members: one subscription, $20 per year, included in dues; Additional Member Subscriptions: $15 per year. Non-Members U.S., Canada, and Mexico: $40 per year, $110 for three years, single copy $15. International Members and Non-Members: $90 per year; $250 for three years; single copy $25. Published by the American Institute of Steel Construction at One East Wacker Drive, Suite 700, Chicago, IL 60601.

Periodicals postage paid at Chicago, IL and additional mailing offices. **Postmaster:** Send address changes to ENGINEERING JOURNAL in care of the American Institute of Steel Construction, One East Wacker Drive, Suite 700, Chicago, IL 60601.

Acknowledgment

All AISC *Engineering Journal* articles are peer reviewed prior to publication for accuracy, content and style. AISC thanks the following engineers for their voluntary review assistance to the *Engineering Journal* Review Board throughout 2008.

Farid Alfawakhiri
American Iron and Steel Institute

Scott F. Armbrust
W & W Steel, LLC

Robert E. Bachman
Consultant

Allan Baker
Berube Leonard, LLC

Peter C. Birkemoe
University of Toronto

Reidar Bjorhovde
The Bjorhovde Group

Mark D. Bowman
Purdue University

Roger L. Brockenbrough
R. L. Brockenbrough & Associates, Inc.

Michel Bruneau
University of Buffalo

Peter J. Carrato
Bechtel Corporation

Janice J. Chambers
University of Utah

Christopher P. Conn
The Harman Group, Inc.

Constantin Christopoulos
University of Toronto

James Davidson
Auburn University

John T. DeWolf
University of Connecticut

Richard M. Drake
Fluor Enterprises, Inc.

Christopher J. Earls
Cornell University

W. Samuel Easterling
Virginia Tech

Edward Egan
Southern Iron Works, Inc.

Bruce R. Ellingwood
Georgia Institute of Technology

Howard I. Epstein
University of Connecticut

Shujin Fang
Sargent & Lundy, LLC

Marshall T. Ferrell
Ferrell Engineering, Inc.

James M. Fisher
Computerized Structural Design, SC

John W. Fisher
Lehigh University

Jean-Marc Franssen
University de Liège

Theodore V. Galambos
University of Minnesota

Maria Garlock
Princeton University

Louis F. Geschwindner
American Institute
of Steel Construction

Lawrence G. Griffis
Walter P. Moore

Subhash C. Goel
University of Michigan

W. Scott Goodrich
Structural Detailing, LLC

Gilbert Grondin
University of Alberta

Jerome F. Hajjar
University of Illinois
at Urbana-Champaign

Ronald O. Hamburger
Simpson Gumpertz & Heger Inc.
Consulting Engineers

Mark V. Holland
Paxton & Vierling Steel Company

John D. Hooper
Magnusson Klemencic Associates

Nestor Iwankiw
Hughes Associates

William P. Jacobs
Stanley D. Lindsey & Associates

Wladyslaw Jaxa-Rozen
Bombardier Inc.

Matthew A. Johann
Ove Arup & Partners

Richard C. Kaehler
Computerized Structural Design, S.C.

Theodore L. Karavasilis
Lehigh University

Michael T. Kempfert
Computerized Structural Design, SC

Lawrence A. Kloiber
LeJeune Steel

Lawrence F. Kruth
Douglas Steel Fabricating Corporation

Geoffrey L. Kulak
University of Alberta

Keith Landwehr
Schuff Steel Company

Barbara Lane
Ove Arup & Partners

LeRoy A. Lutz
Computerized Structural Design, S.C.

Jason P. McCormick
University of Michigan

Robert A. MacCrimmon
Hatch Canada

Murty K.S. Madugula
University of Windsor

James O. Malley
Degenkolb Engineers

John Mattingly
CMC Joist

Saul B. Mednick
Globe Iron Construction Company, Inc.

Ronald Meng
Lynchburg Steel Company, LLC

Keith Mueller
Teng & Associates, Inc.

Larry Muir
Consultant

Thomas M. Murray
Virginia Tech

Jack E. Petersen
Martin/Martin Consulting Engineers

Christopher H. Raebel
Milwaukee School of Engineering

Clinton O. Rex
Stanley D. Lindsey & Associates

James M. Ricles
Lehigh University

Charles W. Roeder
University of Washington

John A. Rolfes
Computerized Structural Design, SC

Rafael Sabelli
Walter P. Moore

Thomas A. Sabol
Englekirk & Sabol, Inc.

C. Mark Saunders
Rutherford & Chekene
Consulting Engineers

Stephen P. Schneider
Kramer Gehlen & Associates Inc.

Clifford W. Schwinger
The Harman Group, Inc.

Robert E. Shaw
Steel Structures Technology Center, Inc.

Donald R. Sherman
Consultant

W. Lee Shoemaker
Metal Building Manufacturers
Association

Emmet A. Sumner
North Carolina State University

Akbar Tamboli
The Thornton-Tomasetti Group, Inc.

William A. Thornton
Cives Engineering Corporation

Raymond H.R. Tide
Wiss Janney Elstner Associates, Inc.

Emile W.J. Troup
Consultant

Chia-Ming Uang
University of California–San Diego

Asif Usmani
University of Edinburgh

Timothy M. Utter
Foster Wheeler North America Corp.

Jules Van de Pas
Computerized Structural Design, S.C.

Michael A. West
Computerized Structural Design, S.C.

Ronald G. Yeager
Steel-Art, Inc.

Design of Unstiffened Extended Single-Plate Shear Connections

LARRY S. MUIR and CHRISTOPHER M. HEWITT

Extended single-plate shear connections (Figure 1) offer many advantages that simplify the construction process. Because the connection to the supported member is moved clear of the support, coping of the supported member is not required and the only fabrication process required for the supported member is drilling or punching. Also, because bolted connections are only used in the connection to the supported member, there is no safety concern over the use of shared bolts through the web of the support. Additionally, in some instances, extended single-plate connections are the only practical solution to a framing problem, such as the case of a member framing into the weak axis of a column with continuity plates.

The rigidity of single-plate connections at the support has always been a gray area. Designers have often been concerned about a considerable, unanticipated moment that could be developed in the connection, which could then result in either a moment delivered to the column that the column has not been designed to resist or a sudden rupture of either the weld or the bolts. Section B3.6a of the AISC *Specification for Structural Steel Buildings,* hereafter referred to as the AISC *Specification,* requires that simple shear connections have sufficient rotational capacity to accommodate the required beam end rotation. This paper will address each of these concerns and will present a general design procedure for extended single-plate shear connections.

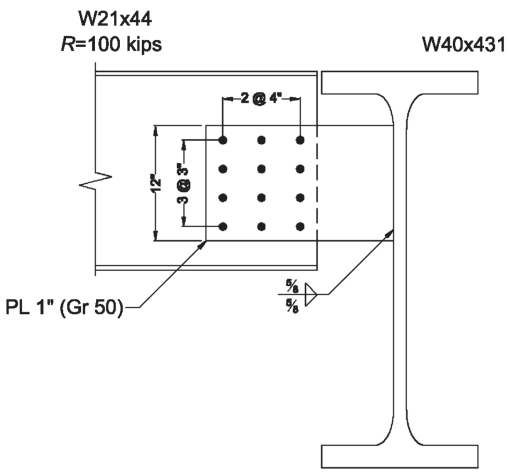

Fig. 1. Extended single-plate shear connection.

This paper outlines the background and development of the design procedure for extended single-plate shear connections presented in the 13th Edition AISC *Steel Construction Manual,* hereafter referred to as the AISC *Steel Manual.* While the method presented in this paper has been determined by the AISC Committee on Manuals and Textbooks to be suitable for all cases, other rational methods may be used at the discretion of the designer.

HISTORY OF USE AND RESEARCH

Extended single-plate shear connections have a long history of use. Illustrations of the use of extended single-plate shear connections have been included in the AISC *Steel Manual* since 1992, and they have been used by designers for several decades. Despite a relatively long history of use, a well-defined, simple and rational design procedure has never been included in the AISC *Steel Manual,* and the design procedure was largely left to the discretion of individual engineers.

Fearing that the plate might buckle or that the weld might fracture, many designers have chosen to detail the connections with top and bottom stiffening plates or to extend the plate and connect it to the top and bottom flanges of a supporting girder (Figure 2). Ironically, testing has shown that extending the plate vertically in this manner could actually result in a lower plate buckling strength (Sherman and Ghorbanpoor, 2002) and is, in many cases, unnecessary.

Sherman and Ghorbanpoor (2002) conducted testing on extended single-plate shear connections and also proposed a design procedure. The procedure is predicated on the use of top stiffening plates and a single column of bolts. The bolts are designed based on an empirically derived eccentricity related to the number of bolts, similar to the contemporary design procedure for conventional single-plate shear connections. Strongly tied to the empirical test data, the procedure does not adequately address the needs of the practicing engineer for all cases.

Larry S. Muir is president, Cives Engineering Corporation, and chief engineer, Cives Steel Company, Roswell, GA.

Christopher M. Hewitt is senior engineer, American Institute of Steel Construction, Inc., Chicago, IL.

ESTABLISHING A MODEL FOR THE CONNECTION DESIGN

A beam connected to a support by a single-plate shear connection is an indeterminate system. The moment applied to the connection will depend on many factors, including the distance that the connection extends from the support and the relative stiffnesses of the supported beam, the connection and the support. Though it might be assumed that the moments at the support are bounded by those predicted by the pinned-end beam model at the low end, and those predicted by the fixed-end beam model at the high end, even this is insufficient. There is a possibility that the support, or connection, at one end of the beam could be quite flexible, while the other end is extremely rigid. In such a case the stiffer end would be subjected to a moment greater than the fixed-end beam moment. The upper bound then becomes the moment developed at the fixed end of a propped cantilever. Even if the stiffnesses of the supports and the beam could be reliably predicted, determining the stiffness of the connection is problematic. Not only must the stiffness of the plate be determined, but factors such as bolt slip and bearing deformation must also be accounted for in order to accurately predict the distribution of the moments in the system.

Without an accurate prediction of the moment distribution, establishing a design procedure for the connection might seem intractable. Fortunately, instead of trying to predict the behavior of the connection in service, an assumed model can be established and then steps can be taken to control the behavior to support the assumptions. This approach is supported by the lower bound (static) theorem, which states:

> If an equilibrium state can be found which does not violate the yield condition, then however 'unlikely' that state may seem to be, the structure is safe. (Baker and Heyman, 1969)

Thus, the applied external forces in equilibrium with the internal force field are less than or, at most, equal to the applied external force that would cause failure, provided that all the limit states are satisfied and sufficient ductility exists to allow redistribution of the forces.

The most logical model to use is the pinned-end beam model (Figure 3) since it replicates the typical assumptions made during the main member design. The pinned-end model assumes that the connection delivers only the shear reaction from the supported beam to the support. Based on this assumption, the bolt group will be subjected to a moment equal to the shear reaction multiplied by the distance from the support to the center of the bolt group.

ANTICIPATED BEHAVIOR

As stated earlier, the lower bound theorem is predicated on sufficient ductility being present to redistribute the loads. To accomplish this, the plate, as the most ductile element in the connection, is used as a fuse to shed unwanted moments prior to rupture of either the bolts or the weld. To describe this behavior the system can be modeled as a fixed-end beam of varying cross section. As the beam is loaded moments will be produced at supports, resulting in a moment diagram similar to Figure 4.

As the load increases, the possibility exists that the connection will be subjected to a moment greater than its yield

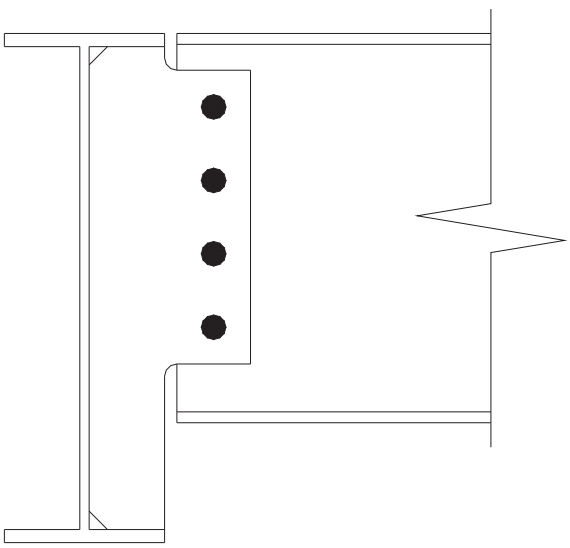

Fig. 2. Single-plate shear connection lengthened to connect to top and bottom flanges of support.

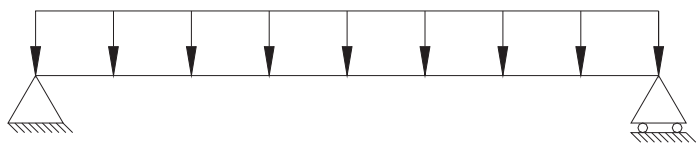

Fig. 3. Simply supported beam model.

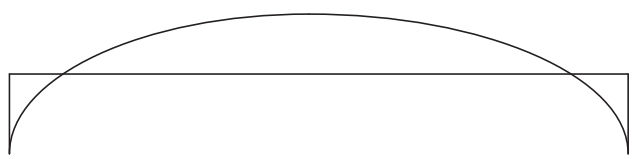

Fig. 4. Moments on a fixed-end beam.

strength. If this occurs, the plate will begin to yield and it will shed the excess moment to the beam, thereby relieving moment from both the connection and the support. The moment distributes to the beam because the yielding of the plate effectively lowers the plate's stiffness. This can be seen by examining the stress-strain curve for steel (Figure 5). When the plate is first loaded its modulus of elasticity, E, is 29,000 ksi. However, as it is loaded beyond the yield stress, the stress-strain curve is no longer linear, and the behavior is better predicted by the tangent modulus of elasticity, E_T, which will be significantly lower than E.

SIZING THE PLATE FOR STRENGTH AND DUCTILITY

In order for the plate to act as a fuse, as described earlier, it must yield without rupturing the bolts or the welds and must possess sufficient strength to support the required loads, thereby setting both a lower and an upper limit on the plate thickness.

Determining the minimum required thickness is straightforward. The limit states of gross shear yielding, net shear rupture, gross flexural yielding, and net flexural rupture all must be satisfied. The plastic section modulus is used in checking both flexural yielding and rupture. This is supported by recent test results (Mohr, 2005). Though not presented as a limit state in the AISC *Specification*, it is recommended that shear and bending interaction be checked. This is done by applying the von Mises yield criterion:

$$\left(\frac{f_v}{\phi_v 0.6F_y}\right)^2 + \left(\frac{f_a}{\phi_a F_y}\right)^2 \le 1.0$$

This can be rewritten in terms of the nominal reaction, R_n, as:

$$\left(\frac{\frac{R_n}{dt_p}}{\phi_v 0.6F_y}\right)^2 + \left(\frac{\frac{4R_n a}{d^2 t_p}}{\phi_a F_y}\right)^2 \le 1.0$$

$$R_n = \frac{F_y dt_p}{\sqrt{2.25 + 16\left(\frac{a}{d}\right)^2}}$$

where

ϕ = 0.90
Ω = 1.67

It should be noted that the current AISC procedure recommends calculating a reduced bending strength related to the applied shear. The AISC approach, also based on the von Mises yield criterion, is theoretically equivalent to the preceding procedure. However, since the AISC equation, $F_{cr} = \sqrt{F_y^2 - 3f_v^2}$, includes both resistance and load terms on the right side of the equation, it may be cumbersome to apply.

Block shear and net shear must also be checked in accordance with Sections J4.3 and J4.2b of the AISC *Specification*.

Additionally, since the edge of the plate in compression may buckle, a stability check must be performed using the relationship (Muir and Thornton, 2004):

$$\phi F_{cr} = 0.90F_y Q$$

where

$Q = 1$ for $\lambda \le 0.7$
$Q = (1.34 - 0.486\lambda)$ for $0.7 < \lambda \le 1.41$
$Q = (1.30/\lambda^2)$ for $\lambda > 1.41$

$$\lambda = \frac{d\sqrt{F_y}}{10t_p\sqrt{475 + 280\left(\frac{d}{a}\right)^2}}$$

If λ is less than or equal to 0.7, the limit state of plate buckling will not control. It is advisable to size the plate to prevent this limit state. However, if plate bucking must be considered as a controlling limit state, it is recommended that the elastic section modulus be used as a conservative method of calculating of the applied bending/buckling capacity of the plate.

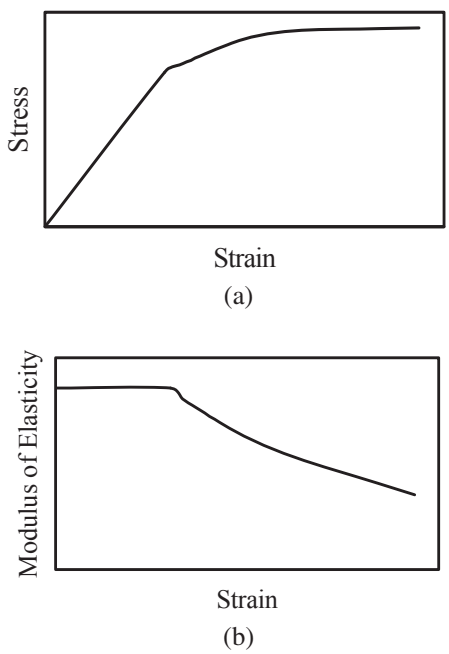

Fig. 5. (a) Stress-strain and (b) modulus of elasticity-strain curves for steel (based on tangent modulus).

Another possible concern is the torsional restraint provided by the extended connection. Most beam designs assume that the beam has full torsional end restraint. In terms of torsional restraint, the extended single-plate shear connection is very similar to a beam coped at the top and the bottom flanges. As with the case of a coped beam, if a slab is present, there should be little concern over the torsional restraint of the connection. However, where torsional restraint is a concern, it can be checked using the procedure presented by the Australian Institute of Steel Construction (Hogan and Thomas, 1988).

The flexural rupture strength of connection elements was investigated by Murray and Mohr (Mohr, 2005). It may be noted that during this testing, a restraining bolt was installed in the plates to prevent buckling prior to developing the full plastic strength of the member. A review of their data indicates that the values for λ varied from a low of 0.538 to a high of 0.685. The preceding theory would not have predicted the buckling in any of the plates. However, there is an important distinction that can be made between the Murray and Mohr tests and extended single-plate shear connections. The Murray and Mohr tests were designed to cause a uniform bending moment on the plates in order to test the moment capacity in the absence of any other factors. It has been shown that for a plate subjected to uniform bending, the critical length at which buckling will occur quickly decreases as the section progressively yields. For nonuniform bending, the decrease is much less pronounced and is negligible for cantilevers. (Baker, Horne, and Heyman, 1956). An extended single-plate shear connection will not be subjected to uniform bending throughout its length and, like a beam designed using the plastic section modulus, will rarely, if ever, experience appreciable yielding in service. Buckling was not a significant problem in either the Murray and Metzger (Metzger, 2006) tests or the Sherman and Ghorbanpoor (2002) tests. Buckling was given as a failure mode for only three of the tests in the Sherman and Ghorbanpoor regime, in two cases where the tab plate was extended to allow welding to the bottom flange of the support beam and a third where it is listed as "a secondary effect of twist" (Sherman, 2002).

As stated previously, the plate acts as a fuse to protect both the bolts and the welds from rupture, thereby allowing the moments to redistribute in an acceptable manner. In order to safeguard the weld, the plate must yield prior to the weld fracturing. Prior to the 13th Edition AISC *Steel Manual*, AISC required that the welds to the support be sized as at least ¾ of the plate thickness. This requirement was developed to ensure that the plate would yield before the weld yielded (Astaneh, 1989). In the latest procedure, this recommendation has been modified, and the new procedure recommends that the plate be sized to yield before the weld ruptures. This is a more logical approach, as weld yield is not a well-defined limit state, and joint separation will not occur until the weld ruptures. The modified requirement calls for the weld be equal to or greater than ⅝ of the plate thickness.

The ⅝ t_p requirement is derived here and was verified by testing (Metzger, 2006), as is discussed later in this paper. In the derivation, the rupture strength of the weld is assumed to be $\sqrt{2/3}F_{EXX}$. This is more conservative than the strength of a transversely loaded fillet weld reflected in the AISC *Steel Manual* of $1.5(0.6)F_{EXX}$, but results in a closed-form solution to the problem. It also matches well with the 2006 American Welding Society (AWS) requirement 2.24.1.3, which is intended to prevent the unzipping of welds at tubular connections. AWS states that the ultimate breaking strength of fillet welds with 60 ksi or 70 ksi tensile strength shall be taken as 2.67 times the basic allowable stress. This results in a stress of 2.67(0.3)(70) = 56.1 ksi compared to $\sqrt{2/3}(70)$ = 57.1 ksi with the more convenient value assumed in this paper to obtain a closed-form solution. William A. Thornton (unpublished) originally proposed this approach prior to the AISC *Steel Manual* adopting an increased strength for transversely loaded fillets. The required weld can also be derived using the strength specified in the AISC *Steel Manual*, but a closed-form solution cannot be obtained (though the solutions bound a somewhat smaller required weld, as would be expected.)

As stated previously, the rupture strength of the weld is assumed to be $\sqrt{2/3}F_{EXX}$. From this, the shear strength on the weld can be calculated as:

$$F_{shear} = \frac{1}{\sqrt{3}}F_u = \frac{1}{\sqrt{3}}\sqrt{\frac{2}{3}}F_{EXX} = \frac{\sqrt{2}}{3}F_{EXX}$$

The interaction equation for the weld is:

$$\left(\frac{R_n}{2\frac{1}{\sqrt{2}}wL_w\frac{\sqrt{2}}{3}F_{EXX}}\right)^2 + \left(\frac{R_n e}{2\frac{1}{\sqrt{2}}w\frac{L_w^2}{4}\sqrt{\frac{2}{3}}F_{EXX}}\right)^2$$

$$= \left(\frac{R_n}{\frac{2}{3}wL_wF_{EXX}}\right)^2 + \left(\frac{R_n e}{\frac{1}{2\sqrt{3}}wL_w^2F_{EXX}}\right)^2 \le 1.0$$

Solving for R_n yields:

$$R_n \le \frac{wL_wF_{EXX}}{\frac{\sqrt{3}}{2}\sqrt{3+16\left(\frac{e}{L_w}\right)^2}}$$

Similarly for the plate, the interaction equation is:

$$\left(\frac{V_u}{V_{np}}\right)^2+\left(\frac{M_u}{M_{np}}\right)^2\le 1.0$$

$$\left(\frac{R_n}{t_pL_w\dfrac{F_y}{\sqrt{3}}}\right)^2+\left(\frac{R_ne}{\dfrac{1}{4}t_pL_w^2F_y}\right)^2\le 1.0$$

Solving for R_n yields:

$$R_n\le\frac{t_pL_wF_y}{\sqrt{3+16\left(\dfrac{e}{L_w}\right)^2}}$$

Since the plate must yield before the weld fractures, the following must be true:

$$\frac{t_pL_wF_y}{\sqrt{3+16\left(\dfrac{e}{L_w}\right)^2}}\le\frac{wL_wF_{EXX}}{\sqrt{\dfrac{9}{4}+12\left(\dfrac{e}{L_w}\right)^2}}$$

Solving for the weld size, w, yields:

$$w\ge\frac{t_pF_y\sqrt{3}}{2F_{EXX}}$$

Assuming F_y = 50 ksi and F_{EXX} = 70 ksi yields:

$$w\ge 0.619t_p\cong\frac{5}{8}t_p$$

In a similar fashion, the plate safeguards the bolt group by yielding prior to bolt shear. To ensure that this takes place, a maximum plate thickness is determined based on the strength of the bolt group. To determine the moment strength of the bolt group, the instantaneous center of rotation method is used. To obtain the maximum moment capacity of the bolt group, a moment-only condition is assumed. The instantaneous center of rotation coincides with the center of gravity of the bolt group and the strength can be calculated as:

$$M_{max}=1.25F_{nv}A_bC'$$

where

$$C'=\sum\left[L_i\left(1-e^{-\left(\frac{10L_i\Delta_{max}}{L_{max}}\right)}\right)^{0.55}\right]$$

It should be noted that the bolt shear strength given in Table J3.2 of the AISC *Specification* includes a 20% reduction to account for the uneven force distribution that occurs in end loaded bolt groups (Kulak, 1987). Since this bolt group is not end loaded, the 20% strength reduction can be neglected. This is the origin of the 1.25 factor preceding the equation. It should also be noted that this is a check to ensure ductility and not strength; therefore, safety factors have not been applied to capacities of either the bolts or the plate. This is similar to the approach used for the weld ductility check shown previously.

Once the moment strength of the bolt group is determined, it can be compared to the flexural yield strength of the plate to obtain a maximum plate thickness:

$$t_{max}=\frac{6M_{max}}{F_yd^2}$$

The elastic section modulus is used in this check because the plate will begin to redistribute stress after first yielding.

SIZING THE BOLT GROUP

Assuming a pinned-end beam model that delivers only shear to the face of the support, the moment that exists on the bolt group can be calculated as:

$$M_{bolt}=Re$$

The strength of bolt group can be calculated in the typical fashion, using the instantaneous center of rotation method. Though the bolt group is not end loaded, the 20% bolt shear strength reduction inherent in the AISC *Specification* cannot be neglected when designing for strength in practice. Accounting for the 20% reduction is a requirement of the AISC *Specification* as currently written, although from a theoretical standpoint the reduction is not necessary in this case.

SUPPORT ROTATION

Resistance of the support against rotation is often questioned when extended single-plate shear connections are used. In the current design procedure, because all of the connecting elements are designed to resist or otherwise accommodate the entire range of anticipated moments, support rotation and connection deformation from the plate and bolts are serviceability and not strength considerations.

When a rigid support condition exists, all significant rotation of the beam end is accommodated by deformation of the plate and the bolt group, and serviceability need not be considered. A rigid support is one in which the support and the connected beam tend to stay in place or rotate in the same direction. A rigid support may generally be assumed in any of the following cases:

Table 1. Vertical Deflections Due to Short Slotted Holes	
n	**Δ**
2	1.06
3	0.526
4	0.350
5	0.262
6	0.209
7	0.174
8	0.149
9	0.131
10	0.116
11	0.104
12	0.095

- The single-plate connection is attached to a column flange.
- Single-plate connections are framed to both sides of a girder or column web.
- A structural slab is present, attaching to both the girder and the beam flanges.
- The torsional resistance of the girder provides sufficient rotational restraint.

If the support is considered flexible, consideration must be given to the serviceable rotation limit for the connection. Serviceability merits greater concern when short slots are used at a flexible support. It should be noted, however, that the rotation allowed even by short slots is limited by the geometry of the connection. For a connection with a single column of bolts, the angle of rotation can be approximated as:

$$\theta = \tan^{-1}\left(\frac{\left(L_s - d_b\right)}{\left(n-1\right)s - 1/16}\right)$$

The vertical deflection caused by the rotation will be approximately equal to:

$$\Delta = \tan\left(\theta\right)e = \frac{e\left(L_s - d_b\right)}{\left(n-1\right)s - 1/16}$$

The resulting vertical deflections, given a 10-in. eccentricity and 1-in.-diameter bolts in short-slotted holes spaced at 3 in., are as listed in Table 1.

Assuming a ¼ in. of deflection can be tolerated, rotation problems do not exist as long as at least five rows of bolts are provided. The limit of ¼ in. is derived from the suitable performance history of standard shear tabs with short-slotted holes, which will result in a theoretical deflection of about 5⁄16 in. With two or more columns of bolts, the additional geometrical restraint reduces the rotation by a factor of 4, effectively eliminating the problem (Figure 6).

In typical cases, the slab, when cured, can provide the necessary resistance to rotation. Prior to curing, the rotation caused by the dead load must be resisted by the bolted connection alone acting as a slip-critical connection. For this reason, if excessive support rotation during erection is a concern, the bolts should be pretensioned and a minimum of a Class A faying surface should be present when short slots are used. It should be noted that the worst case for any serviceability problems is a connection utilizing a single column of bolts with two rows. As either the number of rows or columns of bolts are increased, the rotation allowed by the movement in the holes drops off quickly, so that there would be essentially no problems for any connections with a double column of bolts, and the rotation of connections with single columns of bolts is only a concern when less than about five rows are employed.

The upper bound of the moment to be resisted by the bolts is defined by the design resistance of the connection, which is designed for bearing and factored down to include only the dead load. The required relationship can be written as:

$$\frac{\phi R_{sc} C'}{e} \geq \frac{\phi R_v C}{1 + L/D}$$

The ratio of the slip resistance with a Class A faying surface to the shear strength of an ASTM A325X bolt is approximately:

$$\frac{\phi R_{sc}}{\phi R_v} = \frac{\phi \mu D_u h_{sc} T_b N_s}{\phi F_{nv} A_b}$$

$$= \frac{1.00\left(0.35\right)\left(1.13\right)\left(0.85\right)\left(0.70\right)\left(90\text{ ksi}\right)\pi\left(\frac{d_b}{2}\right)^2 (1)}{(0.75)(60\text{ ksi})\pi\left(\frac{d_b}{2}\right)^2}$$

$$= 0.471$$

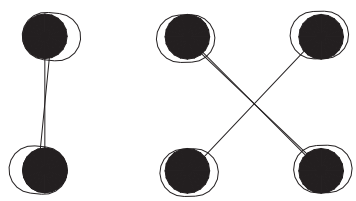

Fig. 6. Rotational restraint provided by (a) single column of bolts and (b) double column of bolts.

It should be noted that in this ratio, the bolt pretension is taken to be 70% of the nominal tensile strength of the bolt instead of the values given in the AISC *Specification*. This is done to provide a closed-form solution to the problem. The ratio for ASTM A490 bolts is similar. It can also be shown that the ratio of C' to C is approximately 10 for eccentricities of 9 to 10 in. From this, a maximum eccentricity, e, can be calculated as:

$$e = \left(1 + L/D\right)0.471(10) = 4.71\left(1 + L/D\right)$$

In the formulation of the original LRFD *Specification*, a live-to-dead load ratio of 3 was assumed. Using the same assumption here results in a maximum eccentricity of 17.8 in. Since this is greater than the typical eccentricity used in practice, the connection will experience no serviceability problems before the concrete is cured, so long as pretensioned bolts are used with a Class A faying surface. Even with a live-to-dead load ratio as low as 1.25, serviceability will not be a problem for eccentricities up to 10 in.

Of course, once the concrete has cured, the connection may be subjected to the full live and dead loading. Serviceability must be considered for this case as well, though a different model can be used. A couple consisting of a tension force at the bolt group and a compression force in the slab will resist the rotation caused by the eccentric gravity loads. Again considering an upper bound defined by the design resistance of the connection in bearing, the required relationship for a bolt spacing of 3 in. is:

$$n\left(\phi R_{sc}\right)\frac{\left(3\text{ in.}\right)n}{2} \geq \phi R_v Ce$$

Again recognizing the ratio of the slip resistance with a Class A faying surface to the shear capacity of an ASTM A325 bolt is:

$$\frac{\phi R_{sc}}{\phi R_v} = 0.471$$

We find that:

$$n^2 \geq 1.4Ce \Rightarrow e \leq \frac{n^2}{1.4C}$$

Table 2. Allowable Eccentricity with Cured Concrete Slab

e—no slab	*C*	*e*—with slab (in.)
2	1.18	2.42
3	0.88	3.25
4	0.69	4.14
5	0.56	5.10
6	0.48	5.95
7	0.41	6.97
8	0.36	7.94
9	0.32	8.93
10	0.29	9.85
12	0.24	11.9
14	0.21	13.6
16	0.18	15.9
36	0.08	35.7

Looking at the worst case, a two-row connection, the resulting eccentricities are shown in Table 2.

Table 2 demonstrates that the eccentricity that can be resisted assuming model (c) in Figure 7 is greater than or equal to the eccentricity that the bolt group would be designed to resist as a bearing connection. Therefore, excessive support rotation and vertical deflections are unlikely to occur in practice when the assumed conditions are met.

The preceding discussion emphasized the effects of support rotation as it applies to an unrestrained support. In such cases, the support is assumed to have no stiffness, and no moment is resisted by the support. The problem is strictly one of serviceability. However, the report issued by Sherman and Ghorbanpoor (2002) addressed a "web mechanism" limit state. The web mechanism was created when the moment resistance of the column was mobilized through deformation of the column web. Since the design procedure in the AISC *Steel Manual* sizes the components to resist the full

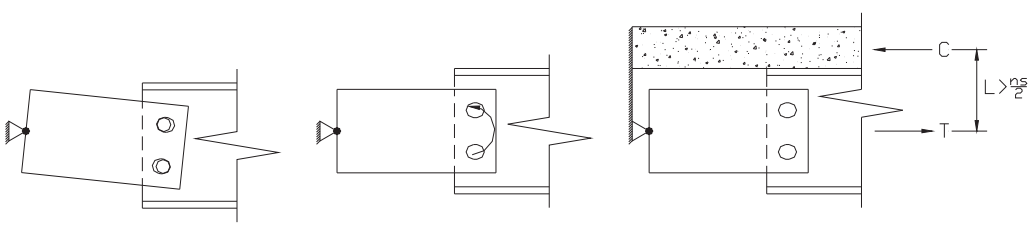

Fig. 7. Support rotation at short slotted holes. (a) Support restrained by bolts slipping into bearing. (b) Support restrained by slip resistance to moment. (c) Support restrained by slip resistance to tension and compression in slab.

eccentricity at the bolted connection, the rotational resistance of the support is not required to resist the design loads. The rotation is therefore limited to the simple beam end rotation (usually assumed to be on the order of 0.03 radian) and the rotation allowed by the bolt slip in the holes and bearing deformations in the plates and the bolts. Since this deformation is self-limiting, it is only a serviceability concern.

The limited rotation that results from the AISC procedure can be seen by examining a plot of shear versus rotation from the Sherman and Ghorbanpoor test 1-U (Figure 8). In this test, the girder rotated more than 9 degrees. This obviously exceeds the rotation predicted by simple beam end rotation and connection slip. However, when the predicted capacity from the AISC *Steel Manual* is shown (represented by the heavy horizontal line), it can be seen that the resulting support rotation is limited to less than 3 degrees. The combined rotation that could be expected from the simple beam end rotation, and the connection slip would be about 4 degrees. Limiting the applied load to the design capacity instead of the nominal capacity would result in a further decrease in the support rotation.

COMPARISON TO TEST RESULTS

There is data available from 13 tests performed on unstiffened, extended single-plate connections. Sherman and Ghorbanpoor (2002) presented the results of eight tests. Murray and Metzger (Metzger, 2006) performed five additional tests sponsored by Cives Steel Company. The plates in seven of the tests conformed to the parameters of the design procedure presented in this paper. However, all of the Sherman tests used a weld equal to ¾ of the plate thickness, and all of the Murray tests used a weld equal to ½ the plate thickness. The objective of the Sherman and Ghorbanpoor project

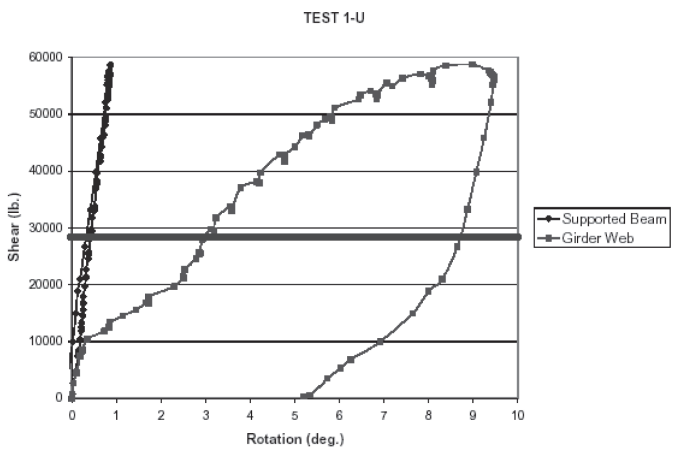

Fig. 8. Plot of shear versus rotation for the Sherman and Ghorbanpoor test 1-U.

was to develop a design procedure for extended single-plate connections. The objective of the Murray and Metzger testing program was to verify the procedures contained in the AISC *Steel Manual* for both conventional and extended single-plate connections. A special emphasis of the Murray and Metzger testing was to validate the reduction in required weld size from ¾ of the plate thickness to ⅝ of the plate thickness. Thus, the available test data represent a wide spectrum of conditions. The single-plate connections in the Sherman testing were all attached to the webs of either columns or girders and are representative of connections with flexible supports, where the bolts would tend to be the more critical than the welds. The Murray single-plate connections were all attached to the flange of a W14×90 and are representative of connections with rigid supports, where the welds would tend to be the more critical than the bolts.

As can be seen in Table 3, the design procedure contained in the AISC *Steel Manual* provides a good margin of safety. Though not typically considered in the design of shear connections, one failure mode emphasized in the work of Sherman and Ghorbanpoor, which is not explicitly considered in the current design procedure, is that of plate twist. Two tests, 2-U and 4-U, are reported as having failed primarily by twisting of the plate.

Work by Bennetts, Thomas, and Grundy (1981) investigated shear connections with the specific goal of developing an understanding of the torsional behavior of shear connections due to the eccentricity of load between the connecting plates and the adjacent beam web. This investigation included testing to determine the torsional stiffness of many types of shear connections, including extended single-plate connections. In that work, the researchers showed that single-plate connections maintain the majority of their torsional rigidity until the plate yields, at which time, as one might expect, the torsional rigidity of the connection decreases and the twist of the connection becomes apparent. To design for this effect, the limit state of twist in the new design procedure is implicitly checked considering the von Mises interaction of forces on the plate, which ensures that the plate does not yield in the presence of shear forces. Effects of twisting can be further mitigated by the lateral bracing of the beam when a slab is present. As can be seen in the test results from Sherman and Ghorbanpoor, the measured capacity was 82.9 kips for test 2-U and 98.7 kips for test 4-U. The limit predicted by the von Mises interaction for both conditions is 85.6 kips, which is accurate to within approximately 3% of the measured capacity of the connection and supports the assumption that twist effects are appropriately addressed by the limit state of yielding of the connection. Twist is listed as a secondary failure mode for tests 6-U and 6-UB, which resisted 138 kips and 136 kips, respectively. The von Mises limit state predicts a capacity of only 116 kips. Further work to refine procedures for considering torsional limit states in all types of shear connections may be appropriate.

Table 3. Summary and Comparison of Unstiffened Extended Single-Plate Connection Test Data												
Test	**Columns of Bolts**	**Rows of Bolts**	**Depth of Plate (in.)**	***a* (in.)**	**Maximum Allowed Plate Thickness (in.)**	**Plate Thickness Provided (in.)**	**Meets Criteria for Extended Shear Tab?**	**Meets Criteria for Standard Shear Tab?**	**Tested Capacity**	**Tested Predicted**	**Tested Design (Factor of Safety)**	**Tested Adj. Design* (Factor of Safety)**
Sherman and Ghorbanpoor												
1-U	1	3	9	6.85	0.402	⅜	YES	NO	58.7	2.08	5.19	4.15
2-U	1	5	15	6.3	0.421	⅜	YES	NO	82.9	1.00	2.51	2.01
3-U	1	3	9	6.86	0.402	⅜	YES	NO	54.8	1.94	4.85	3.88
3-UM	1	3	9	6.86	0.402	⅜	YES	NO	58.6	2.07	5.18	4.15
4-U	1	5	15	10.04	0.421	½	NO	NO	98.7	1.79	4.48	3.59
6-U	1	6	18	10.04	0.428	½	NO	NO	138	1.77	4.43	3.54
6-UB	1	6	18	10.04	0.428	½	NO	NO	135.8	1.74	4.36	3.48
8-U	1	8	24	10.04	0.426	½	NO	NO	173.6	1.31	3.28	2.62
Murray and Metzger												
1	1	3	8.5	3	0.259	⅜	NO	YES	81	1.11	1.85	1.85
2	1	4	11.5	3	0.271	⅜	NO	YES	110	1.48	3.69	2.95
3	1	5	14.5	3	0.259	⅜	NO	YES	146	1.10	2.75	2.20
4	1	7	20.5	3	0.256	⅜	NO	YES	200	1.08	2.70	2.16
5	2	3	8.5	3	0.695	½	YES	NO	89	1.20	2.99	2.39
6	2	5	14.5	3	0.585	½	YES	NO	200	1.18	2.94	2.35
7	1	7	20.5	9	0.256	⅜	YES	NO	97	1.07	2.68	2.14
5A**	2	2	8.5	3	0.368	½	NO	NO	88	2.16	5.39	4.31

* Where bolt shear controls the design value, the 20% reduction for end-loaded connections has been removed.
** Connection failure did not occur.

Plate buckling was not listed as a failure mode for any of the unstiffened, extended single-plate connection tests. Interestingly when the plate was extended to the bottom flange of the supporting girder, as illustrated in Figure 2, the plate was more likely to buckle.

SUMMARY OF RECOMMENDED DESIGN PROCEDURE

The following procedure has been adopted into the AISC *Steel Manual* as a universally applicable method of designing single plate shear connections. A general extended single-plate shear connection is shown in Figure 9. The procedure, referred to as the extended procedure, is useful when the dimensional and other limitations of the conventional single-plate shear connection design method cannot be satisfied. This procedure can be used to determine the strength of single-plate shear connections with multiple vertical rows of bolts.

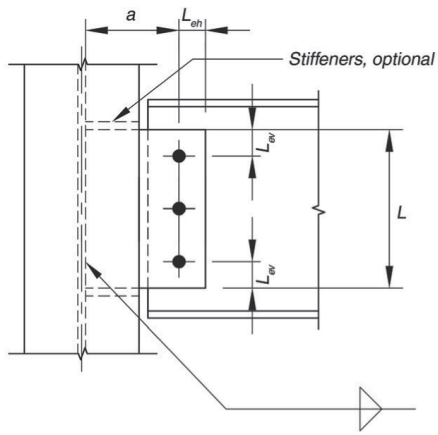

Fig. 9. General extended single-plate connection configuration.

Limitations

1. The use of holes must satisfy AISC *Specification* Section J3.2 requirements. The shear load can be considered to be applied transverse to the slots. The eccentricity does not require that the bolts be designed as slip-critical.

2. The horizontal and vertical edge distances, L_{eh} and L_{ev}, must satisfy AISC *Specification* Table J3.4 requirements.

Design Checks

1. Determine the bolt group required for bolt shear and bolt bearing with eccentricity, *e,* measured as the distance from the support to the center of the bolt group. Alternative considerations of the design eccentricity are acceptable when justified by rational analysis. For example, see Sherman and Ghorbanpoor (2002).

2. Determine the maximum plate thickness permitted such that the plate moment strength does not exceed the moment strength of the bolt group in shear, as follows:

$$t_{max} = \frac{6M_{max}}{F_y d^2}$$

where

M_{max} = $1.25F_v A_b C'$

$1.25F_v$ = shear strength of an individual bolt from AISC *Specification* Table J3.2, ksi, multiplied by a factor of 1.25 to remove the 20 percent reduction for uneven force distribution in end-loaded bolt groups (Kulak, 2002). The joint in question is not end loaded.

A_b = area of an individual bolt, in.^{2}

C' = coefficient from Part 7 of the AISC *Steel Manual* for the moment-only case (instantaneous center of rotation at the centroid of the bolt group), in.

F_y = plate specified yield stress, ksi

d = plate depth, in.

The foregoing check is made at the nominal strength level, since the check is to ensure ductility, not strength.

Exceptions:

a. For a single vertical row of bolts only, the foregoing criterion need not be satisfied if either the beam web or the plate satisfies $t \le d_b/2 + 1/16$ and both satisfy $L_{eh} \ge 2d_b$.

b. For a double vertical row of bolts only, the foregoing criterion need not be satisfied if both the beam web and the plate satisfy $t \le d_b/2 + 1/16$ and $L_{eh} \ge 2d_b$.

3. Check the plate for shear yielding, shear rupture and block shear rupture.

4. Check the plate for flexure with the von Mises shear reduction. That is, check the available flexural yielding strength of the plate, ϕM_n or M_n/Ω, based upon a critical stress F_{cr}:

$$F_{cr} = \sqrt{F_y^2 - 3f_v^2}$$

$$M_n = F_{cr} Z$$

$$\phi = 0.90 \qquad \Omega = 1.67$$

These equations can be rearranged to be directly solvable in terms of the connection available strength as ϕR_n or R_n/Ω such that

$$R_n = \frac{F_y d t_p}{\sqrt{2.25 + 16\left(\frac{a}{d}\right)^2}}$$

$$\phi = 0.90 \qquad \Omega = 1.67$$

5. Check the plate for buckling.

6. Size weld as $w = 5/8 t_p$

7. Ensure that the supported beam is braced at points of support.

8. Check serviceability criteria.

The design procedure for extended single-plate shear connections permits the column to be designed for an axial force without eccentricity. In some cases, economy may be gained by considering alternative design procedures that allow the transfer of some moment into the support, for example, 5% of the beam fixed-end moment, provided that this moment is also considered in the design of the supporting member.

To provide for stability during erection and lateral support of the beam, it is recommended that the minimum plate length be one-half the *T*-dimension of the beam to be supported. The maximum length of the plate must be compatible with the *T*-dimension of an uncoped beam and the remaining web depth, exclusive of fillets, of a coped beam. Note that the plate may encroach upon the fillet(s) as shown in Figure 10-3 of the AISC *Steel Manual*.

DESIGN EXAMPLE

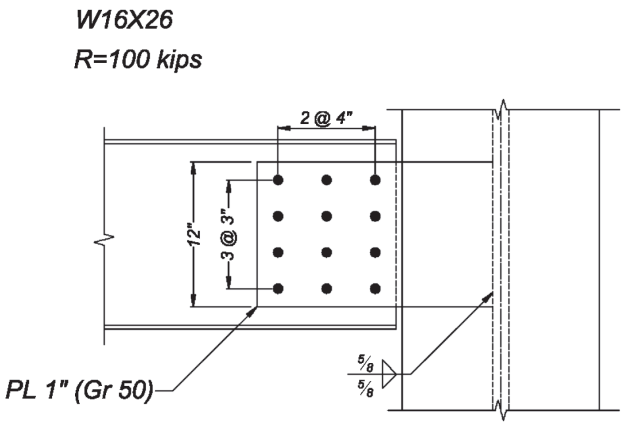

Consider a W16×26 with a 100 kip (LRFD) end reaction (see figure). Find an extended single-plate shear connection to support the end reaction.

Assume 1-in. diameter ASTM A490-N bolts (ϕR_v = 35.3 kips/bolt), a = 9.5 in., and all edge distances equal to 1.5 in.

Determine the equivalent bolt strength of the bolt group.

$C = 3.44$

Maximum strength of bolt group due to bearing

$$R = \phi 2.4 F_u t_w d_b$$

$$= (0.75)(2.4)(65 \text{ ksi})(0.25 \text{ in.})(1.0 \text{ in.})$$

$$= 29.3 \text{ kips/bolt}$$

Determine required C-value

$$C_{req'd} = \frac{R_u}{\phi R_{n/bolt}} = \frac{100 \text{ kips}}{29.3 \text{ kips}} = 3.41 \le 3.44 \quad \textbf{o.k.}$$

The check, however, will be performed to demonstrate the calculations involved. Find maximum plate thickness such that plate will yield before bolts rupture by accounting for the 20% reduction in bolt strength generally applied to account for the case of end-loaded connections.

$$R_n = \frac{\phi R_v}{(1-0.20)\phi} = \frac{35.3 \text{ kips}}{0.8(0.75)} = 58.8 \text{ kips/bolt}$$

Find the "pure moment" strength of the bolt group (Many conditions are tabulated in the AISC *Steel Manual* Part 7, in Tables 7-7 through 7-14)

$$C' = 4(6.02)\left(1 - e^{-10(0.34)}\right)^{0.55} + 2(4.5)\left(1 - e^{-\left(\frac{10(4.5)(0.34)}{6.02}\right)}\right)^{0.55} + 4(4.27)\left(1 - e^{-\left(\frac{10(4.27)(0.34)}{6.02}\right)}\right)^{0.55} + 2(1.5)\left(1 - e^{-\left(\frac{10(1.5)(0.34)}{6.02}\right)}\right)^{0.55}$$

$C' = 50.7$ in.

The moment strength of the bolt group is therefore,

$$M = C' R_n = 50.7 \text{ in.}(58.8 \text{ kips}) = 2{,}980 \text{ kip-in.}$$

Determine the maximum plate thickness. Note that the elastic section modulus is used because the plate will begin to redistribute stress after first yielding.

$$t_{max} = \frac{6M}{F_y d^2} = \frac{6(2{,}980 \text{ kip-in.})}{50 \text{ ksi}(12 \text{ in.})^2} = 2.48 \text{ in.}$$

Try a 1-in.-thick plate with F_y = 50 ksi.

Check shear and bending interaction on gross plate section (von Mises criteria)

$$\phi R_n = \frac{\phi F_y d t_p}{\sqrt{2.25 + 16\left(\frac{a}{d}\right)^2}}$$

$$= \frac{0.90(50 \text{ ksi})(12 \text{ in.})(1 \text{ in.})}{\sqrt{2.25 + 16\left(\frac{9.5 \text{ in.}}{12 \text{ in.}}\right)^2}} = 154 \text{ kips}$$

Check net shear rupture on the plate

$R_n = 0.6 F_u A_{nv} = 0.75(0.6)(65 \text{ ksi})(7.5 \text{ in.}^2)$

$= 219 \text{ kips} > 100 \text{ kips}$ **o.k.**

Check block shear rupture on the plate

$\phi R_n = \phi F_u A_{nt} U_{bs} + \min(\phi 0.6 F_y A_{gv}, \phi 0.6 F_u A_{nv})$

Tension rupture component

$\phi F_u A_{nt} U_{bs}$ = 0.75(65 ksi)(6.69 in.)(1 in.)(0.5) = 163 kips

Shear yielding component

$\phi 0.6 F_y A_{gv}$ = 0.75(0.6)(50 ksi)(10.5 in.)(1 in.) = 236 kips

Shear rupture component

$\phi 0.6 F_u A_{nv}$ = 0.75(0.6)(65 ksi)(6.56 in.)(1 in.) = 192 kips

R_n = (163 kips + 192 kips) = 355 kips 100 kips **o.k.**

Check plate buckling

$$\lambda = \frac{d\sqrt{F_y}}{t_p\sqrt{47{,}500 + 112{,}000\left(\frac{d}{2e'}\right)^2}}$$

$$= \frac{12\sqrt{50}}{1\sqrt{47{,}500 + 112{,}000\left(\frac{12}{2(9.5)}\right)^2}} = 0.279 < 0.7$$

Buckling does not control.

Size the weld to ensure that the plate will yield before the weld ruptures:

$w = 0.625 t_p = 0.625(1) =$ ⅝ in.

SYMBOLS

a = the distance from the face of the support to the first vertical line of bolts

c = number of column (vertical rows) of bolts

d = plate depth

d_b = bolt diameter

e = the distance from the face of the support to the center of the bolt group

f_a = the applied bending stress (net or gross)

f_v = the applied shear stress (net or gross)

n = the number of rows

s = the spacing between rows of bolts

t_p = plate thickness, in.

w = weld leg size, in.

A_b = area of bolt, in.^{2}

C = coefficient for eccentrically loaded bolt groups, from AISC *Steel Manual* Part 7.

C' = coefficient used in determining the equivalent pure-moment bolt group strength

D = live load

E = modulus of elasticity, ksi

E_T = tangent modulus of elasticity, ksi

L = live load

F_{EXX} = electrode classification number, ksi

F_{nv} = the shear strength of an individual bolt from AISC *Specification* Table J3.2, ksi

F_y = the minimum specified yield stress, ksi

F_u = the minimum specified tensile stress, ksi

L_i = the distance of the ith bolt from the center of gravity of the bolt group

L_{max} = the distance of the bolt furthest from the center of gravity of the bolt group to the center

L_s = the length of the slot

L_w = length of weld, in.

R = the simple beam end reaction

ϕR_{sc} = the slip resistance provided by a single bolt as a serviceability limit state

ϕR_{brg} = the shear capacity of a single bolt

Δ = vertical deflection caused by the rotation of bolts in short slotted holes

Δ_{max} = the maximum deformation on the bolt furthest from the center of gravity, 0.34 in.

λ = slenderness parameter, dimensionless (Young's modulus is incorporated in formula)

θ = rotation allowed by movement in short slotted holes

REFERENCES

AISC (2005), *Specification for Structural Steel Buildings*, ANSI/AISC 360-05, American Institute of Steel Construction, Chicago, Illinois.

AISC (2005), *Steel Construction Manual*, 13th Edition, American Institute of Steel Construction, Chicago, Illinois

AWS (2006), Structural Welding Code—Steel, AWS D1.1/D1.1M:206, American Welding Society, Miami, Florida.

Astaneh, A., Call, S.M. and McMullin, K.M. (1989), "Design of Single-Plate Shear Connections," AISC, *Engineering Journal,* 1st Quarter, pp. 21–32.

Baker, J.F., Horne, M.R. and Heyman, J. (1956), *The Steel Skeleton: Volume II Plastic Behavior and Design,* The Syndics of the Cambridge University Press, Cambridge.

Baker, J.F. and Heyman J. (1969), *Plastic Design of Frames,* The Syndics of the Cambridge University Press, Cambridge.

Bennetts, I.D., Thomas, I.R. and Grundy, P. (1981), "Torsional Stiffness of Shear Connections," *Proceedings of the Metal Structures Congress,* National Committee on Metal Structures of the Institution of Engineers, Australia, Newcastle, N.S.W., May 11–14, pp. 102–106.

Hogan, T.J. and Thomas, I.R. (1988), *Design of Structural Connections*, 3rd Edition, Australian Institute of Steel Construction.

Kulak, G.L., Fisher, J.W. and Struik, J.A.H. (1987), *Guide to Design Criteria for Bolted and Riveted Joints*, 2nd Edition, John Wiley, New York.

Metzger, K.A.B. and Murray, T.M. (2006). "Experimental Verification of a New Single Plate Shear Connection Design Model," Masters Thesis, Virginia Tech, Blacksburg, VA.

Mohr, B. and Murray, T.M. (2005). "Investigation of Ultimate Bending Strength of Steel Bracket Plates." Masters Thesis, Virginia Tech, Blacksburg, VA.

Muir, L.S. and Thornton, W.A. (2004), "A Direct Method for Obtaining the Plate Buckling Coefficient for Double-Coped Beams," *Engineering Journal*, AISC, 3rd Quarter, pp. 133–134.

Neal, B.G. (1977), *Plastic Methods of Structural Analysis,* 3rd edition, Taylor and Francis, London.

Sherman, D.R. and Ghorbanpoor, A. (2002), "Design of Extended Shear Tabs," American Institute of Steel Construction Final Report, University of Wisconsin-Milwaukee.

Experimental Evaluation of the Influence of Connection Typology on the Behavior of Steel Structures Under Fire

ALDINA SANTIAGO, LUIS SIMÕES DA SILVA, PAULO VILA REAL, GILBERTO VAZ and ANTÓNIO GAMERIO LOPES

The behavior of steel joints under fire loading is a subject that has only recently received special attention by the research community. In fact, as recently as 1995, the European pre-standard on the fire response of steel structures (CEN, 1995) deemed it unnecessary to assess the behavior of steel joints under fire conditions. This approach was supported by the argument that there is increased thermal mass at the joint area. However, observations from real fires show that, on several occasions, steel joints fail, particularly their tensile components (such as bolts or end plates), because of the high cooling strains induced by the distortional deformation of the connected members (Bailey, Lennon and Moore, 1999; Buchanan, 2002; Wald, Simões da Silva, Moore, Lennon, Chladna, Santiago, Benes, and Borges, 2006a).

The experimental results on the response of steel joints under fire conditions are relatively recent and limited, partly because of the high cost of fire tests and the limitations on the size of furnace used. The primary aim of these few fire tests was concentrated on obtaining the moment-rotation relationships of isolated joints and the test procedure followed the testing of isolated joints at room temperature (Lawson, 1990; Leston-Jones, 1997; Al-Jabri, 1999). Despite the importance of such tests, they do not reflect the behavior of a complete structure under an urban fire. Unlike room temperature conditions, joint behavior cannot be adequately represented by a moment-rotation relationship alone. Many aspects of behavior occur due to the interaction between members, and system behavior cannot be predicted or observed in tests of isolated elements. Large variable axial forces combined with bending moment and shear force are induced in the connection as experimentally shown (Allam, Fahad, Liu, Burgess, Plank and Davies, 1999; Liu, Fahad and Davies, 2002). Furthermore, another aspect that should be considered in the study of real structures is the cooling phase of a natural fire and the inherent unloading effects on the structure. During this phase, the plastically deformed beam contracts significantly and some connection components experience tensile forces (Simões da Silva, Santiago, Vila Real and Moore, 2005).

Obtaining detailed experimental evidence of the behavior of steel members subjected to realistic fire conditions is quite difficult and expensive. Natural fire tests, such as the Cardington tests (Simões da Silva et al., 2005) are ideal as they reproduce reality very closely, but it is quite difficult to obtain detailed measurements of the mechanical response of individual members and to quantify the various parameters that control their behavior. To overcome the limitations of isolated member tests and avoid the complexity of fire tests on real structures, carrying out tests on steel subframes constitutes a good compromise. These allow the observation of the redistributions of forces that take place throughout the fire and, in a suitable installation, allow the reproduction of the transient temperature conditions that occur along the length of the members, including the proper consideration of the cooling phase.

The main objective of this paper is to describe an experimental test program carried out by the Department of Civil Engineering at the University of Coimbra on a steel subframe in order to evaluate the behavior of various types of steel joints under a natural fire and transient temperature conditions along the length of the beam. The tests were carried out on a purposely developed experimental installation that could reproduce the transient temperature conditions measured in the seventh Cardington test (Wald, Chladná, Moore, Santiago and Lennon, 2006b). The results of these tests provide invaluable evidence on how to design joints that are able to survive a fire.

Aldina Santiago is professor, department of civil engineering, University of Coimbra, Coimbra, Portugal.

Luis Simões Da Silva is professor, department of civil engineering, University of Coimbra, Coimbra, Portugal.

Paulo Vila Real is professor, department of civil engineering, University of Aveiro, Aveiro, Portugal.

Gilberto Vaz is professor, department of mechanical engineering, ISEC—Polytechnic Institute of Coimbra, Coimbra, Portugal.

António Gamerio Lopes is professor, department of mechanical engineering, University of Coimbra, Coimbra, Portugal.

DESCRIPTION OF THE EXPERIMENTAL PROGRAM

General Description

The experimental program consists of the testing of a series of subframes composed by two thermally insulated HEA300 (similar to W12×65) cross-section columns and an unprotected noncomposite IPE300 (similar to W12×26) cross-section beam with 5.70 m (18.7 ft) free span, supporting a concrete slab (Figure 1). These dimensions were chosen to reproduce the measured dimensions of a steel subframe from the fire compartment of the seventh Cardington fire test (Wald et al., 2006a). The steel grade specified for the beam and columns is S355 and the beam cross-section is class 1 at room temperature as well as at elevated temperatures, i.e., compact shape, with adequate ductility for large plastic rotation and development of plastic moment (CEN, 2005a). The slab construction was of steel deck and light weight in-situ concrete composite floor and was intended to reproduce the thermal boundary condition in typical composite frames.

The steel subframe was supported by two reaction frames (Figure 1) perpendicular to the plane of the frame. They provided pinned supports at the top of the columns, allowing free axial movement; the bottom of the columns was hinged and fixed to a reinforced concrete footing that was secured

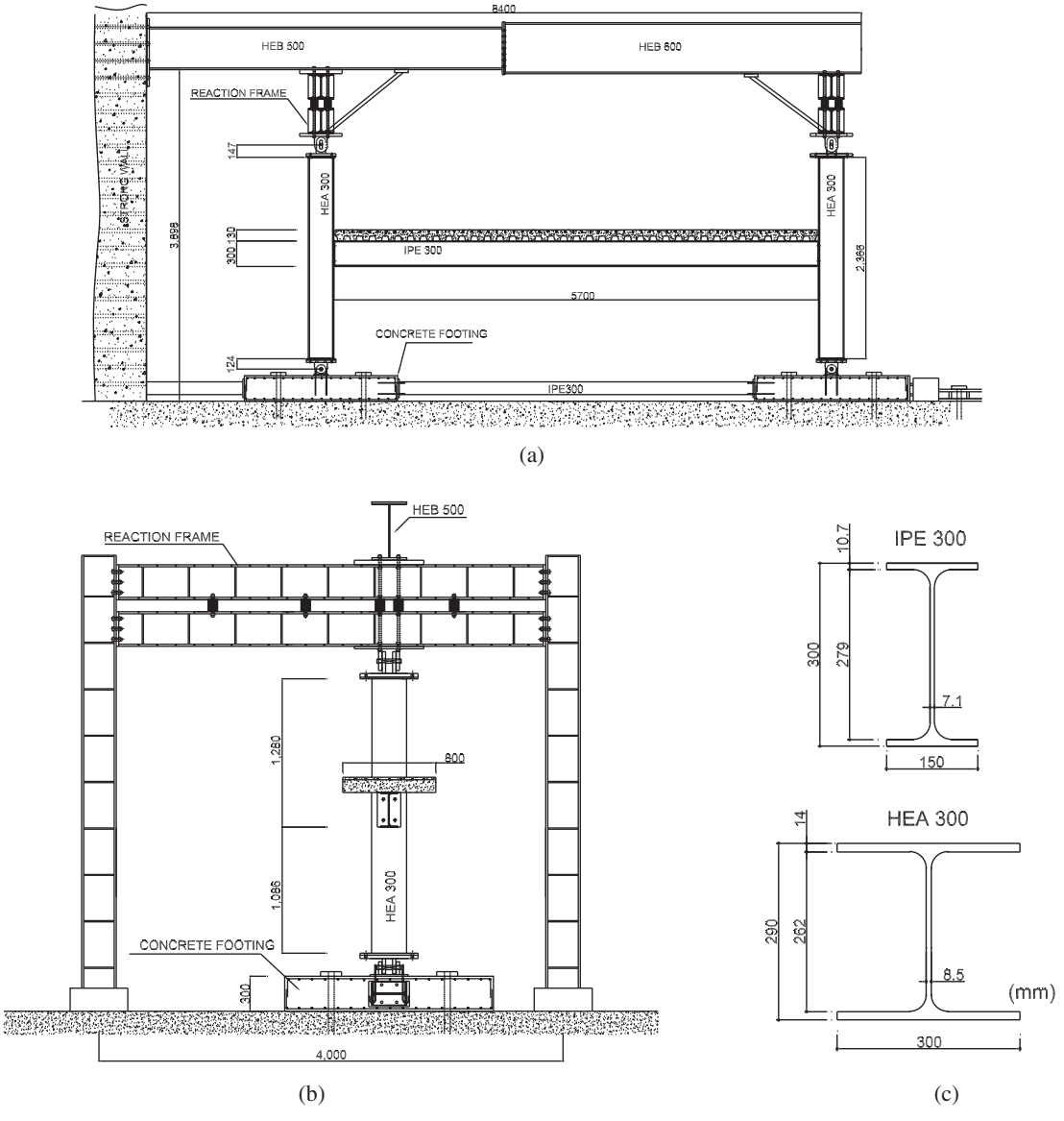

Fig. 1. General layout: (a) longitudinal view; (b) lateral view; (c) geometry of the profiles (1 in. = 25.4 mm).

Table 1. Test Program				
Test ID	**Joint Typology**	**End plate Dimensions (mm) and Steel Grade**	**Bolts / Weld**	**Resistance**
FJ01	Flush end plate	(320×200×10); S275	2 bolt row M20, 8.8	$M_{j,Rd}$ = 47.6 kN-m (42.1 lbf-in.)
FJ02		(320×200×16); S275	2 bolt row M20, 10.9	$M_{j,Rd}$ = 93.0 kN-m (82.3 lbf-in.)
FJ03		(320×200×16); S275	2 bolt row M20, 8.8	$M_{j,Rd}$ = 88.6 kN-m (78.4 lbf-in.)
EJ01	Extended end plate	(385×200×16); S275	3 bolt row M20, 8.8	$M_{j,Rd}$ = 146.6 kN-m (130 lbf-in.)
HJ01	Header plate	(260×150×8); S275	4 bolt row M20, 8.8	$V_{j,Rd}$ = 395.4 kN (88,900 lbf)
WJ01	Welded joint	—	$a_f = a_w$ = 10 mm (0.394 in.)	$M_{j,Rd}$ = 147.0 kN-m (130 lbf-in.)

Note: Bolt class 8.8 (f_y = 92,824 psi; f_u = 116,030 psi); bolt class 10.9 (f_y = 130,533 psi; f_u = 145,037 psi); bolt size M20 (nominal size: 0.787 in); steel S275 (39,900 psi); steel S355 (51,500 psi).

in position by Dywidag bars passing through the laboratory strong floor and fixed horizontally using a steel profile connecting both reinforced concrete footings.

The two reaction frames were horizontally restrained at the top by connecting HEB 500 and HEB 600 profiles to the strong wall (Figure 1a). In order to avoid parasitic rotations at the top of the reaction frames and, consequently, mistakes in the measurements, bracing struts were positioned between the top of the reaction frames and the top beam acting as longitudinal bracing.

Lateral movement of the beam was prevented. The beam top flange was restrained at three points: at midspan, at 1500 mm (59.1 in.) to the left side from the midspan, and at 1500 mm to the right side from the midspan. The restraint system is illustrated in Figure 2 and vertical sliding movement is allowed.

Experimental Program

The experimental program was comprised of six tests and the varied parameter was the beam-to-column connection configuration (Table 1). They were representative of usual joint typology used in building frames: header plate, flush and extended end plate; and welded (Figure 3). According to EN 1993-1-8, WJ01, FJ01, FJ02, FJ03 and EJ01 joints are

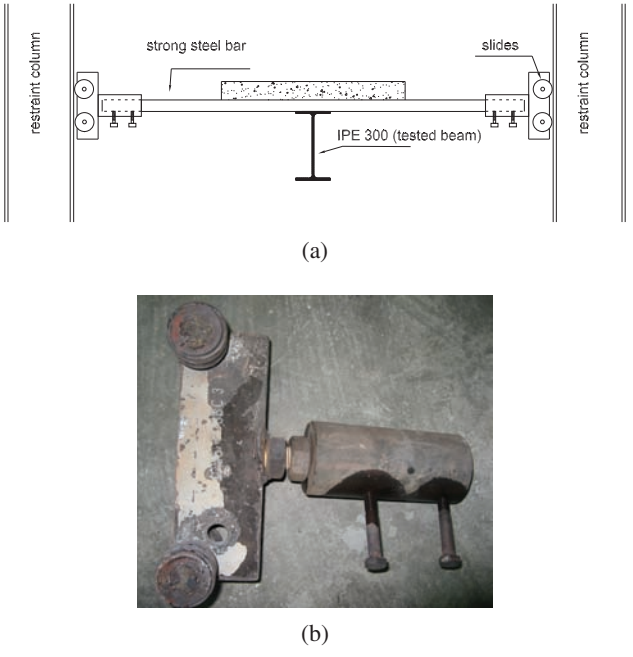

Fig. 2. (a) Lateral restraint system; (b) Detail of slide.

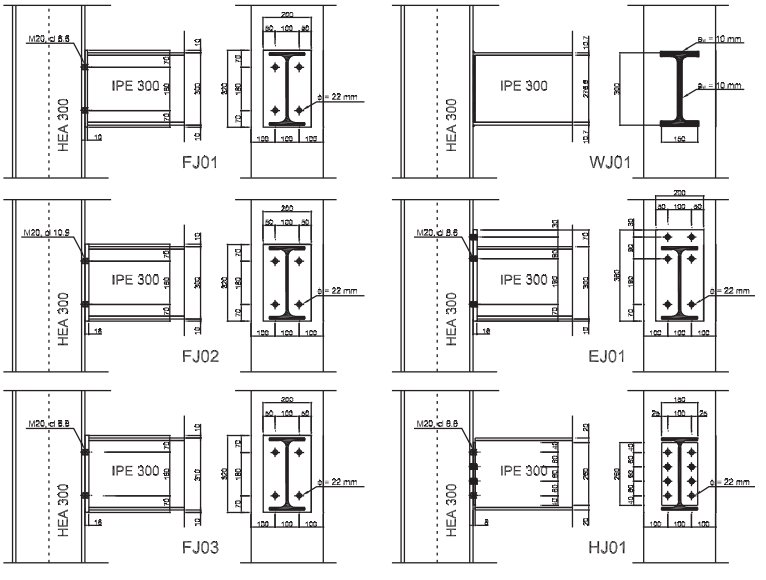

Fig. 3. Geometry of the joints (1 in. = 25.4 mm).

Table 2. Chemical Composition of the S355J2G3 Steels							
% maximum	C	Mn	SI	P	S	N	CEV
IPE 300	0.08	1.02	0.18	0.02	0.022	0.011	–
HEA 300	0.11	1.24	0.21	0.015	0.018	0.011	0.365

Table 3. Mechanical Properties of the Structural Steel S355J2G3											
No. of tests	θ, ºC	$E_{a,\theta}$, GPa	$k_{E,\theta}$	$f_{p,\theta}$, MPa	$k_{p,\theta}$	$f_{y,\theta}$, MPa	$k_{y,\theta}$	$f_{u,\theta}$, MPa	$k_{u,\theta}$	$\varepsilon_{u,\theta}$, %	Z_θ, %
4	20	210	1.00	382	0.99	388	1.01	494	1.00	30.8	63.2
2	100	192	0.91	412	1.06	374	0.96	490	0.99	24.9	66.9
2	200	189	0.90	347	0.90	439	1.15	571	1.15	15.5	52.5
3	300	177	0.84	283	0.73	392	1.03	570	1.15	21.8	48.8
3	400	168	0.80	254	0.66	361	0.95	478	0.97	18.4	52.1
3	500	124	0.59	218	0.56	318	0.83	371	0.75	19.2	39.3
2	600	105	0.50	176	0.45	215	0.56	222	0.45	16.0	27.5
2	700	39	0.19	85	0.22	118	0.31	147	0.30	27.4	73.4
3	800	18	0.09	41	0.11	48	0.13	51	0.10	37.1	37.2
2	900	2	0.01	23	0.06	48	0.12	37	0.07	23.7	18.8
3	1000	1	0.00	18	0.07	27	0.05	29	0.06	21.8	18.0
Note: 1 psi = 6895 MPa; ºF = 1.8(ºC) + 32											

Table 4. Characteristic Values for the Bolts at Room Temperature									
No. of tests	Bolts	E, GPa		f_y, MPa		f_u, MPa		ε_u, %	
		μ	COV %	μ	COV %	μ	COV %	μ	COV %
6	8.8	211.2	2.8	657.7	7.7	834.2	1.8	1.42	25.6
3	10.9	211.6	1.0	860.0	0.2	1078.7	0.2	1.30	32.2
Note: 1 psi = 6895 MPa.									

classified as partial strength and semi-rigid joints while the HJ01 joint is pinned (CEN, 2005b).

Mechanical Properties

Tensile Tests of the Steel Coupons

The test program included two different steel grades: S275 for the end plates (to match the Cardington Frame) and S355 for the steel sections. According to the European Standard EN 10025-1 (CEN, 2004), the steel qualities are S275JR and S355J2G3, respectively. Table 2 summarizes the chemical composition according to the supplied steel certificates.

The steady-state tests of the steel coupons extracted from the profiles were performed according to EN 10002-5 procedures (CEN, 1992). Each test specimen was heated up to a specific temperature and subsequently a tensile test was carried out. The relevant values are set out in Table 3. For each temperature, Young's modulus, E_a, the yield and ultimate stresses, f_y and f_u, the ultimate strain, ε_u, and the coefficient of area reduction, Z, are given. In addition, Table 3 includes the calculated values of the reduction factor for the slope of the linear elastic range $k_{E,\theta} = E_{a,\theta}/E_a$; the reduction factor for effective yield strength $k_{y,\theta} = f_{y,\theta}/f_y$; and the reduction factor for ultimate strength $k_{u,\theta} = f_{u,\theta}/f_u$. No coupon tests were carried out for the end plate material. Coupon tests showed that yield and ultimate stresses first decrease with increasing temperature and then increase at the temperature range of 200 to 300 ºC (392 to 572 ºF) before decreasing at higher temperature. Such behaviors are attributed to the dynamic strain aging (DSA), austenite to martensite transformation, and high-temperature softening in addition to the tempering of bainite. These results show a good comparison with EN 1993-1-2-2005 and with the results obtained by other authors, as described by Santiago (2008).

Tensile Tests of the Bolts

Two different classes of M20 bolts were used in the experiments, 8.8 and 10.9. Several bolts from each group were tested in tension in order to determine the mechanical properties of the bolt material at room temperature. The average properties, μ, and the corresponding coefficient of variation, COV, are set out in Table 4.

Loading Definition

Mechanical Loading

The mechanical loading was applied at two points of the top flange of the noncomposite beam, 700 mm (27.6 in.) to either side of the beam midspan. Each concentrated load was equal to 20 kN (4,500 lbf), which corresponds to a live load ratio of 0.2. The load ratio is here defined as the ratio of the live load at fire limit state [$M_{fi,d}$ = 46 kN-m (40.7 lbf-in.)] to the load-carrying capacity as a simply supported beam at room temperature [M_{Rd} = 223 kN-m (197 lbf-in.) based on a yield stress of 355 MPa (51,500 psi)]. This mechanical loading was applied using two pairs of concrete blocks at room temperature (Figure 4).

Thermal Loading

Thermal loading was applied to the beam and joints (from the beam side only). In order to prevent global structural instability, the columns were thermally protected by 1.18 in. of ceramic fiber blanket [λ = 0.06 W/m-K or 0.035 Btu/(ft-h-°F) at θ = 200 °C or 392 °F; λ = 0.27 W/m-K or 0.156 Btu/(ft-h-°F) at θ = 1000 °C or 1832 °F], where λ denotes the coefficient of thermal conductivity for two different temperatures). Thermal loading was time dependent (heating and cooling phases) and was also variable along the beam span. The tested beams were divided into three heating zones: zone 1 (central zone), and zones 2 and 3 (end zones) (Figure 5). The beam temperature-time curves applied at each beam zone reproduced the values measured in a previous full-scale test (Wald et al., 2006a; Wald et al., 2006b) and they correspond to the measured temperatures at the beam bottom flange. Figure 5b illustrates the prescribed temperature-time curves for the three zones as well as the measured Cardington curve at midspan. The first 10 min of the full-scale fire were neglected because the corresponding temperatures were very low and difficult to reproduce (corresponding to ignition and prior to flashover). For safety reasons, the maximum temperature applied in the tests was 900 °C (1652 °F) at the beam bottom flange (35 min < t < 50 min).

Heating and Exhaust System

To apply the fire load, a special purpose heating system was developed—Natural Fire Facility (Santiago, Simões da Silva and Vila Real, 2008). This heating system consisted of 11 individual gas burners suspended along the beam span. The burners were fitted with externally controlled continuous

(a) (b)

Fig. 4. General layout: (a) preparation; (b) during a fire test.

valves that controlled each zone individually and allowed specifying the range of the flame intensity, and thus reproduce the thermal load strategy (Figure 6). At the same time, control thermocouples at each zone were installed to measure instantaneously the temperature inside the steel. The gas delivered to the system was adjusted by comparing the thermal load strategy with the instantaneous temperature at each control thermocouple. The burners were fed by propane gas through flexible copper pipes (to allow adjustments at the support structure) and were supplied by a battery of gas reservoirs located outside the laboratory. Propane gas allows a definition of a yellow turbulent diffusion flame, common in urban fires. The main reasons this heating system was preferred to a furnace or an electric blanket were the possibility to achieve a direct heating by flame, allowing an easy control of the local thermal load; as the facility is open to the surroundings, a natural convection cooling flow is obtained and the overall setup is easier; and the temperature gradient along the beam is similar to what is observed in an urban fire, as already discussed.

In order to reduce the heat losses to the surroundings and the air entrainment to the vicinity of the beam, rock wool panels were fixed vertically from the exhaust system to the floor. The internal face of the rock wool was aluminized to reflect radiation (Figure 4). This way, the beam heated up not only because of direct incidence of flames but also through radiation from flames, and from the exhaust system and rock wool panels.

In order to allow the exhaust of smoke and combustion gases, the system shown in Figure 4 was used. This exhaust system, fixed to the supporting structure, consists of a semi-circular steel shell around the top of the composite slab and closed at the ends. This semi-circular steel shell drove the combustion gases through flexible steel pipes to a ventilator that forced out these gases to the outside of the laboratory through an opening in the roof.

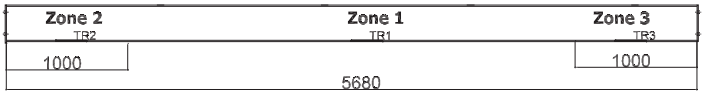

(a)

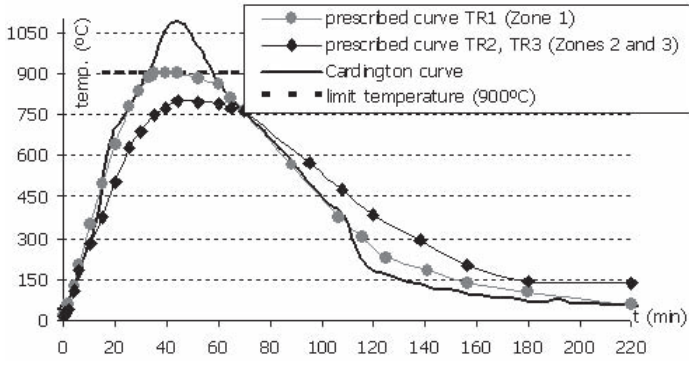

(b)

Fig. 5. Thermal loading: (a) definition of heating zones; (b) steel time-temperature curves of beam bottom flange.

(a)

(b)

(c)

Fig. 6. (a) Individual gas burner; (b) heating system; (c) temperature control system.

Instrumentation

The results were recorded by means of the following instrumentation: thermocouples, displacement transducers and thermographic cameras. Roughly 75 thermocouples of K type with two 0.5-mm (0.02-in.) wires were positioned inside the steel to monitor the temperature in the connected elements (end plate and bolts) and the temperature profiles across the beam and protected columns. The exact number of thermocouples depends on the joint geometry. In order to avoid the direct contact with the flames, the thermocouples attached to the heated beam and the connections were protected by ceramic rods (Figure 7).

Displacement transducers were used to measure displacements and deformations of the beam and columns. They measured beam deflection at mid-span and 300 mm (11.81 in.) away from the joints; horizontal movement of the columns external column flange at the level of the beam axis and the external column flange at the top and bottom ends; and residual displacements of the reaction frame. In the beam, measurements were made outside the fire zone using refractory glass, with a very low thermal expansion coefficient, and a sheaves system that bring the measurements out of the fire zone. A pair of 200-mm (7.87-in.) displacement transducers located at the mid-span of the beam was used to measure the maximum deflection (2×200 mm).

Testing Procedure

The natural fire tests were transient tests. The testing procedure is characterized in two different and sequential steps. In step 1, the mechanical load was applied instantaneously and measurements were recorded. In step 2, the heating unit was switched on. The mechanical loading was maintained constant and the thermal load was incremented according to the prescribed fire strategy.

TESTS RESULTS

Efficiency of the Natural Fire Facility

Figure 8 compares the prescribed fire curves (control system) with the temperatures measured at the beam reference points (TR1, TR2 and TR3) for test EJ01. Good agreement was observed. Similar results were observed for the other five tests.

Temperature

Beam Temperature

Figure 9 depicts the temperature distribution across the beam mid-span cross section for test EJ01. Temperature measurements at mid-span of the beams were taken in the bottom flange (both sides), web and top flange. During the heating phase, the web and bottom flange temperatures are quite similar, despite the fact that the flames surround the bottom flange earlier, the reduced web thickness allowing a faster temperature increase. In the cooling phase, the web temperature decreases faster than the bottom flange temperature for the two following reasons: the reduced thickness corresponds to a lower thermal inertia; and during this phase, the length of flames reduces, and, from a certain moment in time onwards, they only surround the bottom flange. Because of the thermal inertia of the slab and its flame protection effect, the top flange showed the lowest temperature during the

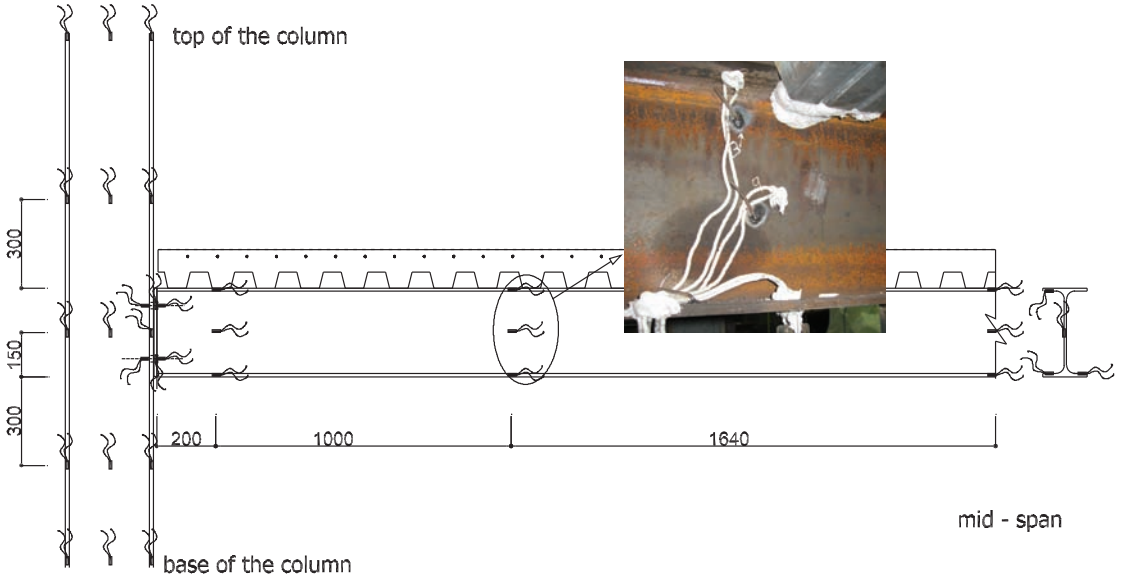

Fig. 7. Location of thermocouples and detail of thermocouples in the beam.

Table 5. Temperatures at Beam Mid-span									
Test Location		Temperature (ºC)							
		15 min.	25 min.	40 min.	50 min.	60 min.	70 min.	80 min.	150 min.
FJ01	bottom flange	454	711	877	878	815	721	619	171
	web	346	694	878	873	801	669	538	144
	top flange	253	505	770	813	780	669	566	226
FJ02	bottom flange	493	730	896	886	867	753	647	183
	web	400	725	872	864	847	645	552	150
	top flange	(a)	(a)	(a)	(a)	(a)	(a)	(a)	(a)
FJ03	bottom flange	499	740	911	908	867	774	680	178
	web	423	730	871	852	792	680	568	162
	top flange	309	588	797	826	810	735	629	206
EJ01	bottom flange	452	727	890	898	845	710	605	152
	web	374	774	882	867	771	623	518	133
	top flange	231	555	763	785	769	677	571	178
HJ01	bottom flange	489	733	882	(b)	(b)	(b)	(b)	(b)
	web	394	718	845	(b)	(b)	(b)	(b)	(b)
	top flange	245	554	743	(b)	(b)	(b)	(b)	(b)
WJ01	bottom flange	478	732	904	914	888	784	679	166
	web	423	726	868	866	829	719	599	158
	top flange	326	613	787	813	815	733	614	208
Average	bottom flange	477	729	893	897	857	748	646	170
	web	393	728	869	864	808	667	555	149
	top flange	273	563	772	809	793	704	595	204
COV %	bottom flange	4.2	1.3	1.4	1.5	2.9	3.9	4.7	6.4
	web	7.5	3.5	1.5	0.8	3.3	4.9	4.9	7.1
	top flange	12	7.1	2.8	1.0	1.8	3.5	3.7	7.7
(a) not measured; (b) beam failure.									

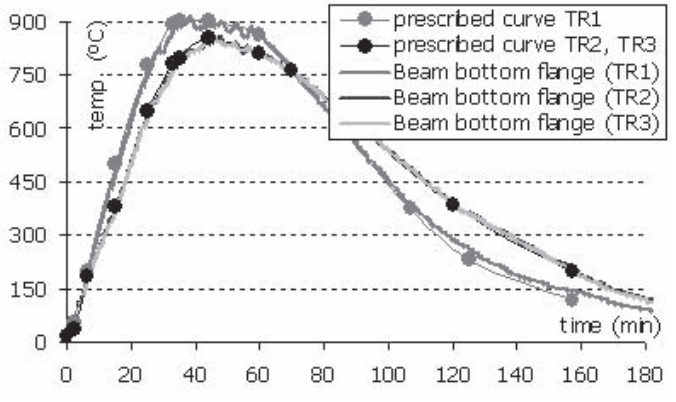

Fig. 8. Measured beam temperature versus prescribed fire curves (test FJ01).

heating phase with a maximum temperature of about 743 °C (1370 °F) and slower cooling, and the maximum top flange temperature was recorded during the cooling phase. Figure 10 was obtained using a thermographic camera. It illustrates the temperature distribution in the central zone of the beam during the heating phase. Table 5 summarizes the temperatures across the depth of the beams; for each test, three different cross-sections were measured: mid-span; at 1650 mm (65 in.) to the Z3 side from the mid-span; and at 1650 mm to the Z2 side from the mid-span. All tests showed similar temperature development during the fire. The average coefficient of variation, COV, is about 4.2%, while the maximum COV does not exceed 12%.

Joint Temperature

Figure 11 compares the temperature-time variation across the depth of the beam 200 mm (7.9 in.) away from the connection Z3 with the bottom flange temperature at mid-span (test EJ01). During the heating phase, the joint temperature was significantly lower than the mid-span bottom flange, which is usually the critical element that defines the limiting temperature of the beam. In contrast, the cooling down in the joint was slower, in accordance with what happens in a real fire situation (Wald et al., 2006b). The maximum temperature near the joints was measured in the bottom flange and corresponded to about 90% of the maximum temperature at mid-span.

Table 6 summarizes the temperatures across the depth of the beams 200 mm (7.9 in.) away from the face of the columns in zones Z2 and Z3. All tests show similar temperature development during the fire. The average coefficient of variation is about 3.6%, while the maximum coefficient of variation does not exceed 9.8%.

Figure 12 compares the temperature curves for the various connection elements of joints in zone Z3 (test EJ01). Measurements were made for each bolt row as follows: in the bolt (beam side); in the bolt shank under the nut (column

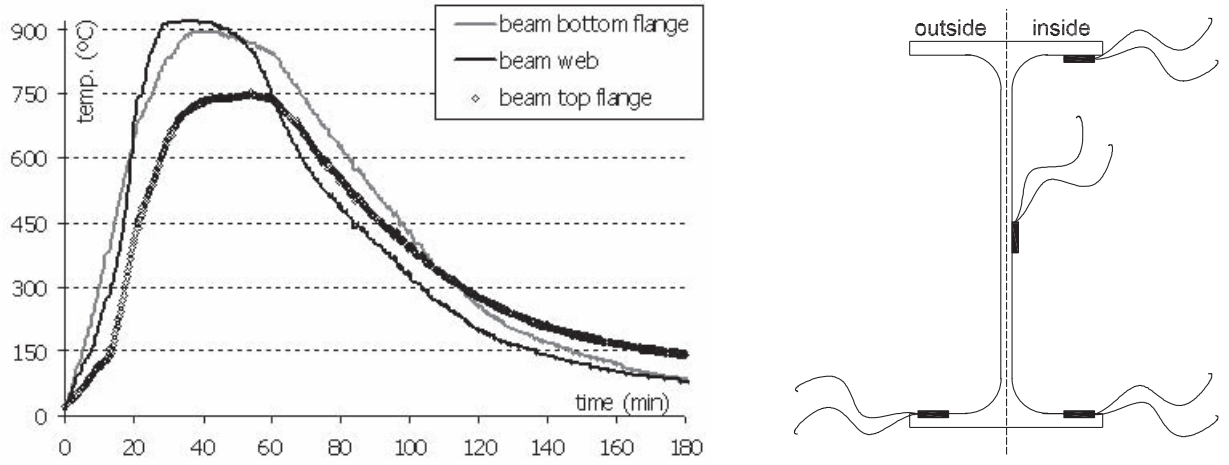

Fig. 9. Temperature distribution across the beam mid-span (test EJ01).

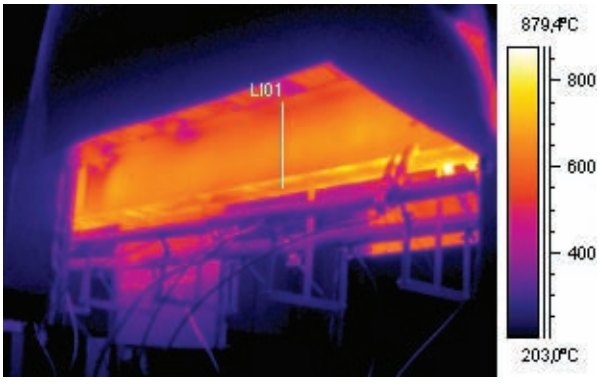

Fig. 10. Thermographic image of the temperature distribution in the beam during the heating phase.

Table 6. Temperatures at Beam Near the Connection (200 mm)									
Test Location		Temperature (°C)							
		15 min.	25 min.	40 min.	50 min.	60 min.	70 min.	80 min.	150 min.
FJ01	bottom flange	326	563	778	821	793	745	670	242
	web	290	587	788	790	735	635	540	206
	top flange	199	424	703	752	742	655	569	247
FJ02	bottom flange	359	612	751	784	783	748	677	234
	web	269	620	738	752	751	702	590	178
	top flange	195	453	666	672	687	687	607	256
FJ03	bottom flange	352	643	842	841	804	766	701	249
	web	298	599	783	782	731	670	589	215
	top flange	214	520	746	752	713	664	596	258
EJ01	bottom flange	379	660	841	847	813	761	686	236
	web	301	632	811	798	745	674	577	200
	top flange	202	555	763	764	720	670	593	241
HJ01	bottom flange	371	638	827	(b)	(b)	(b)	(b)	(b)
	web	269	560	737	(b)	(b)	(b)	(b)	(b)
	top flange	206	470	681	(b)	(b)	(b)	(b)	(b)
WJ01	bottom flange	363	615	822	836	798	753	684	236
	web	300	578	788	786	750	685	585	203
	top flange	191	472	731	750	715	674	592	246
Average	bottom flange	358	622	810	826	798	754	683	239
	web	288	596	774	781	742	673	576	200
	top flange	201	482	715	738	715	670	591	249
COV, %	bottom flange	5.2	6.0	5.1	2.6	1.1	1.2	1.6	2.2
	web	5.2	4.5	3.9	2.0	1.1	3.3	3.2	6.1
	top flange	4.1	9.8	5.3	4.5	2.4	1.6	2.1	2.6
(b) beam failure									

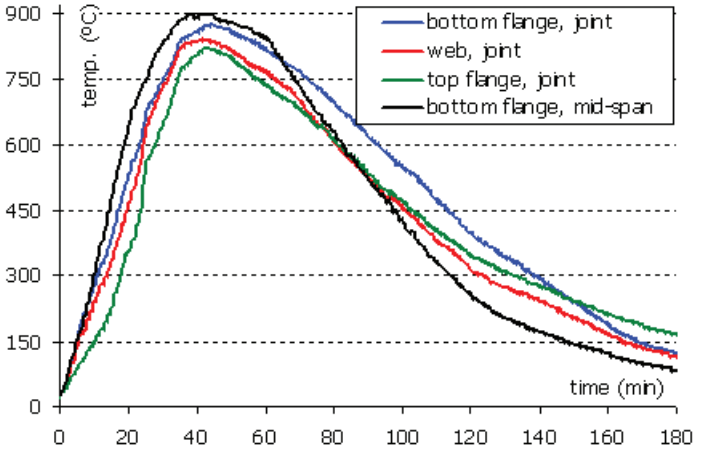

Fig. 11. Temperature in the beam near the joint Z3 (test EJ01).

side); and in the end plate at the same level of the bolt. Again, in the heating phase, the connection temperature was significantly lower than the remote bottom flange at mid-span; in contrast, the cooling down in the joint elements was slower, because of thermal inertia of the adjacent column and connection elements, and the different prescribed thermal loading applied at the joints section. The maximum temperature at the connection is thus reached during the cooling phase.

The first bolt row from the top was significantly cooler than the lower bolts, because the adjacent slab prevents the direct contact from the flames. Furthermore, the thermal inertia of the adjacent column acts as a heat sink. The end plate temperature was quite similar to that of the bolts head at the same level. Exception is made at the level of the second bolt row; in this case, the flames engaged the plate thermocouple more than the bolt head thermocouple and the end plate received more heat than the bolt head. This measurement should not be considered as representative of the average plate temperature at this level. Temperature gradient along the bolts was also measured: the maximum temperature in the head of the third bolt row was about 150 to 200 °C (302 to 392 °F) higher than the corresponding shank; a maximum temperature of about 400 °C (752 °F) was measured in the shanks. For the first bolt row, a difference of about 60 °C (140 °F) on the maximum temperature is observed; this difference could be due to the temperature variation within the beam cross section. The effect of the heat transfer by conduction on the joint element is also evident: the bolt heads and plate heat up first, followed by the corresponding shanks.

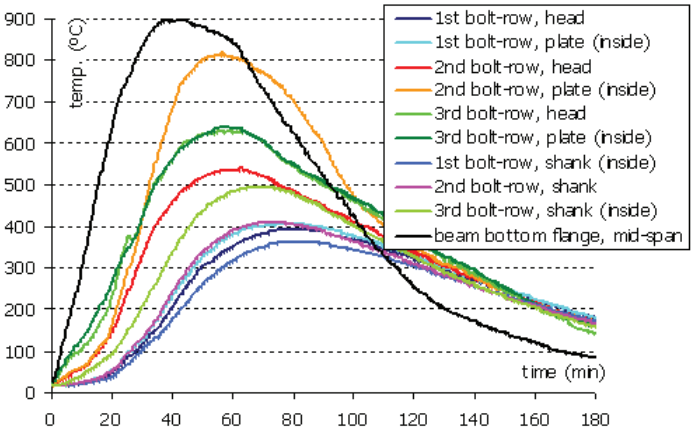

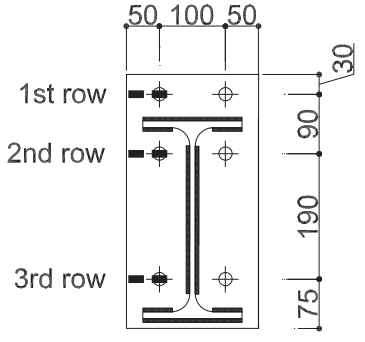

Fig. 12. Temperature within the joint Z3 (test EJ01).

Structural Deformation

Figure 13 compares the evolution of the mid-span deflections during the fire. Most of the beams were able to sustain the load with reduced deflection up to 10 min [$\theta_0 < 150$ °C (302 °F)]; during this stage, the deflection was mainly due to the mechanical loading. Beyond that, due to the loss of stiffness, the midspan deflection increased gradually. Beyond 20 min, a further rise in temperature [$\theta_0 > 550$ °C (1022 °F)] led to a progressive run-away of the beam deflection as the loss of stiffness and strength accelerated. In the case of the FJ02, EJ01 and WJ01 tests, a maximum deflection of 375 mm (14.8 in.) was approximately reached (these values were measured already during the cooling phase). For the HJ01 test, Z3 joint collapsed during the heating phase of the fire [$\theta_0 = 900$ °C (1652 °F)] as a result of the run-away deflection at high temperatures [$\delta_{beam} = 393$ mm (15.5 in.)]. Once the cooling phase started, the heated beams began to recover strength and stiffness from an inelastic state, together with a reduction of thermal strains. This induced tensile, axial forces and the reversal of the deflection. Because of the limited range of the displacement transducers (400 mm), FJ01 curve was incomplete; however, a maximum deflection of 428 mm (16.9 in.) was measured at the end of the fire.

For the same reason, the maximum deflection at the mid-span of beam FJ03 was not measured, but during the cooling phase the deflection reduced to values lower than 400 mm

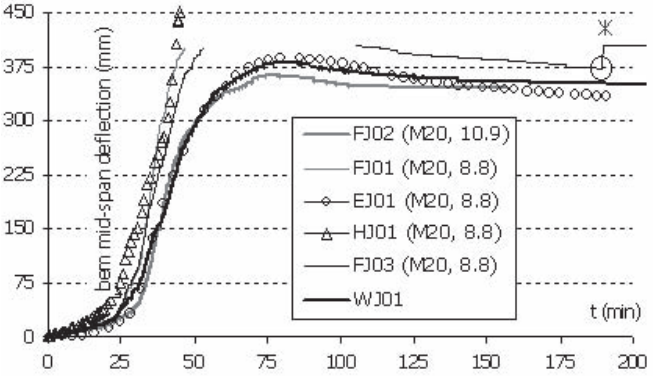

Fig. 13. Mid-span deflection of the beams.

(15.7 in.); moreover, it was possible to identify the failure of the bottom bolt row at t = 190 min after the beginning of the fire; the top bolt row fractured later (t = 382 min). Figure 14 shows the deformed structure at the end of the FJ01 test.

Based on the vertical displacement measured 300 mm (11.8 in.) away from the column end plate surface, d_{z3}, the joint rotation, ϕ, is defined as:

$$\phi = \alpha + \left(\theta_b - \theta_c\right) = \tan^{-1}\left(\frac{d_{Z3}}{300}\right) \quad (1)$$

where α is the contribution from the shear deformation of the column web, and $(\theta_b - \theta_c)$ the change in angle between the centerlines of the beam and column. In these tests, the column hardly deforms as it behaves as a rigid element. Then, both α and θ_c, are neglected. Figure 15 shows the corresponding rotation curves.

Fig. 14. Deformed structure after test FJ01.

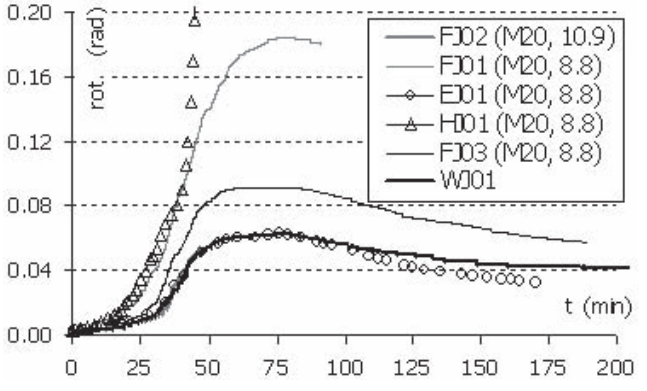

Fig. 15. Joint rotation.

Failure Modes

The six subframe tests revealed distinct behaviors depending on the joint detail. In general terms, one configuration collapsed during the heating phase (HJ01) and three others during the cooling phase (FJ02, FJ03 and EJ01), although in the latter case it was possible to stop the test prior to complete collapse because of safety reasons. The main failure modes observed in the joints of the tested structures are described next.

Test FJ01

Deformation of the end plate was observed, accompanied by local buckling of the beam bottom flange and shear buckling of the beam web (Figure 16). The deformation at the top of the end plate was mainly observed during the heating phase, while deformation at the bottom developed during the cooling phase, due to the tensile force in this zone. Bearing failure of the end plate around the bolts, particularly near the top flange, was also observed. Bolts did not suffer any damage. This failure mode was not surprising due to the reduced thickness of the end plate [10 mm (0.39 in.)].

Test FJ02

Failure modes were apparently similar to those observed for test FJ01: end plate deformation accompanied by local buckling on the beam bottom flange and shear buckling of the beam web (Figure 17a). The end plate deformation was smaller than for test FJ01, because of a thicker end plate [16 mm (0.63 in.)]. However, a clear difference was noted, in the form of nut stripping of the bolts (Figure 17b). This indicated a clear change in failure modes, whereby the bolts became critical in tension during cooling, despite being class 10.9.

Fig. 16. Joint deformation at test FJ01.

Test FJ03

During the heating phase, local buckling on the bottom flange and shear failure at the web were noticed. At the same time, and due to the large joint bending moment, end plate deformation at top developed and the weld on the top flange was broken (Figure 18b). During cooling and due to the large tensile forces that developed during this phase, minor cracks on the weld at the bottom flange (both joints) were observed together with bolt failure in joint Z2 (Figure 18a). The bolt failure mode was by nut stripping: after 190 min. from the beginning of fire, the bottom bolt row fails while the top bolt row broke later (t = 382 min).

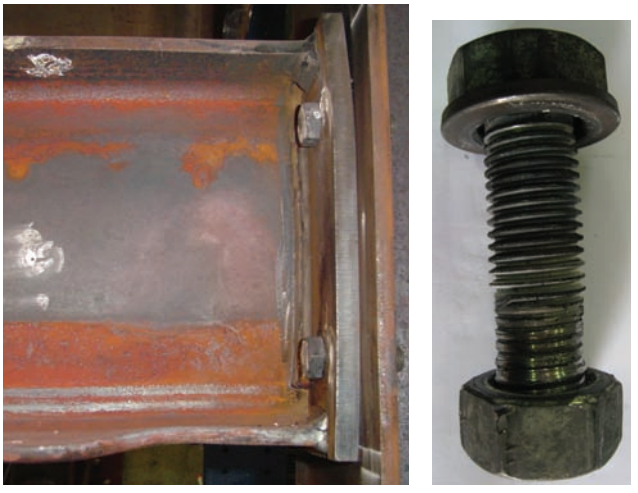

(a) (b)

Fig. 17. (a) End plate deformation; (b) bolt stripping at FJ02.

Test EJ01

During the heating phase, due to the end plate thickness of 16 mm (0.63 in.) and the connection configuration (three bolt rows), no significant end plate deformation developed; only deformation of the beam was observed: local buckling of the beam bottom flange and shear buckling of the beam web. However, during the cooling phase and due to the large tensile forces developed during this phase, localized deformation at the bottom of the end plate and failure (nut stripping) of the bottom bolt row was observed (Figure 19).

Test HJ01

During the heating phase, local buckling on the bottom flange was observed; shear failure at the beam web was insignificant. At the maximum joint temperature of 850 °C (1,562 °F), the end plate broke along both beam web welds (joint Z3), because its tensile resistance is low and it had considerable rotation before the beam and column flange came into contact (Figure 20a). Rapidly, the beam suffered a large deflection, and shear forces were developed near the joint Z2, leading to beam rupture (Figure 20b). No damage to the bolts was observed. This failure mode was not observed in the other bolted joint, because they exhibit larger bending resistance.

Test WJ01

During the heating phase, local buckling on the bottom flange was observed; shear failure at the beam web was minor (Figure 21). No damage to the welds was observed.

Furthermore, other failure modes were observed in the beam and in the concrete slab: shear buckling of the beam web near the load points; bursting of the concrete slab; large

(a) (b) (c)

Fig.18. (a) End plate deformation; (b) bolt stripping;
(c) weld failure at test FJ03 (view from the top of the beam).

(a) (b) (c)

Fig. 19. (a) Local buckling on the beam bottom flange and web; (b) deformation at the bottom of the end plate; (c) nut and bolt stripping—bottom bolt row at test EJ01.

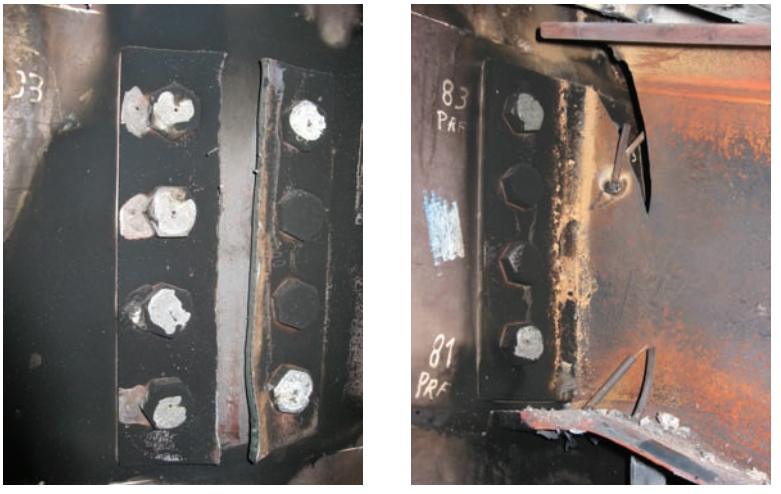

Fig. 20. (a) End plate failure (joint Z2); (b) beam failure (joint Z3) at test HJ01.

Fig. 21. Local buckling on the beam bottom flange and shear buckling of the beam web (joint Z2).

Table 7. Temperature Distribution Across the Depth of the Beam at Mid-span									
Test Location		Temperature (ºC)							
		15 min.	25 min.	40 min.	50 min.	60 min.	70 min.	80 min.	150 min.
Average	bottom flange	477	729	893	897	857	748	646	170
	web	393	728	869	864	808	667	555	149
	top flange	273	563	772	809	793	704	595	204
Thermal gradients	bottom flange	θ_0	θ_0	θ_0	θ_0	θ_0	θ_0	θ_0	θ_0
	web	0.82 θ_0	1.00 θ_0	0.97 θ_0	0.96 θ_0	0.94 θ_0	0.89 θ_0	0.86 θ_0	0.88 θ_0
	top flange	0.57 θ_0	0.77 θ_0	0.86 θ_0	0.90 θ_0	0.93 θ_0	0.94 θ_0	0.92 θ_0	1.21 θ_0
θ_0 = temperature of the bottom flange at beam mid-span									

cracks on the concrete slab due to the separation of the shear studs from the concrete slab; major cracks perpendicular to the slab that occurred as a result of the beam and joints deformation (Figure 22). Due to the considerable size of the columns, column deformations are irrelevant.

DISCUSSION

According to part 1-2 of Eurocode 3 (CEN, 2005c), the beam temperature is calculated as an average temperature within the cross-section that depends on the section factor and the temperature profile is assumed constant within the cross-section. These tests highlight the validity of this simplification adopted by the Eurocode, but only at elevated temperatures; at low temperature ($t < 25$ min and $t > 80$ min) the temperature profile is variable (Figure 23). Based on the temperatures measured along the beam span, the temperature profiles as well as the thermal gradients, linked to different phases of the fire, could be calculated at the mid-span of the beam (Table 7). At low temperatures, the temperature profile is approximately linear and decreases from the bottom to the top flange. As the temperature increases, the temperature in the web increases at a faster rate and the profile becomes convex. At high temperatures, the top flange remains at a lower temperature, while the bottom flange and web show similar values. Finally, during the cooling phase, the temperature profile changes from convex to concave and the top flange now exhibits the highest temperature.

Similarly, based on the temperatures measured near the joints [200 mm (7.9 in.)], temperature profiles and thermal gradients linked to different stages of the fire are calculated where all temperatures are related to the bottom flange

(a) (b)

Fig. 22. Shear buckling of the beam web near the load points.

Table 8. Temperature Distribution Across the Depth of the Beam Near the Joint										
Test Location		Temperature (ºC)								EN 1993-1-2
		15 min.	25 min.	40 min.	50 min.	60 min.	70 min.	80 min.	150 min.	
Average	bottom flange	358	622	810	826	798	754	683	239	
	web	288	596	774	781	742	673	576	200	
	top flange	201	482	715	738	715	670	591	249	
Thermal gradients	bottom flange	0.75 θ_0	0.85 θ_0	0.91 θ_0	0.92 θ_0	0.93 θ_0	1.01 θ_0	1.06 θ_0	1.41 θ_0	0.88 θ_0
	web	0.60 θ_0	0.82 θ_0	0.87 θ_0	0.87 θ_0	0.87 θ_0	0.90 θ_0	0.89 θ_0	1.18 θ_0	0.75 θ_0
	top flange	0.43 θ_0	0.66 θ_0	0.79 θ_0	0.82 θ_0	0.83 θ_0	0.89 θ_0	0.92 θ_0	1.49 θ_0	0.62 θ_0
θ_0 = temperature of the bottom flange at beam mid-span.										

temperature at mid-span, for the same time (Table 8). The experimental results show that the thermal gradient is not constant during a fire, changing from convex to concave with time. Figure 24 illustrates the proposed temperature gradients of EN 1993-1-2 (CEN, 2005c) that only depend on the beam height. It can be seen that the proposed Eurocode thermal gradients approximate the experimental results in the range 20 min < t < 40 min, which corresponds to a bottom flange temperature of circa θ_0 = 830 ºC (1,526 ºF).

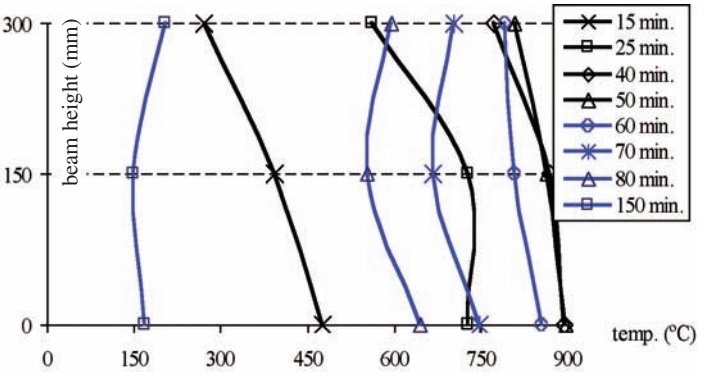

Fig. 23. Temperature profiles across the depth of the beam near the joint.

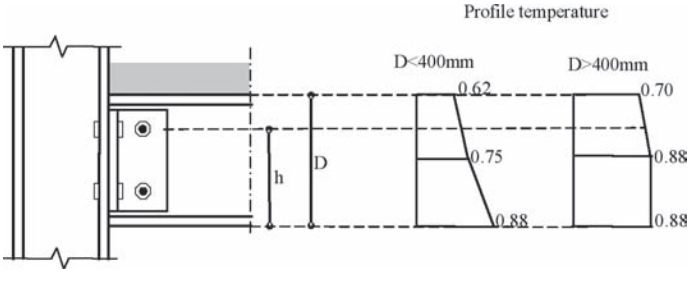

Fig. 24. Thermal gradient across the depth of a composite joint (CEN, 2005c).

Based on the measured axial and vertical displacements of the beam and the axial stiffness of the beam and end restraints, it is possible to estimate the axial force in the beam and the bending moment at the joints. Figures 25 and 26 illustrate the variation of the axial force and bending moment with time.

It can be seen that the joints are subjected to a varying axial force and bending moment throughout the fire event, from an initial state of pure bending. This complex stress state, combined with the M-N resistance interaction diagram for a given temperature profile in the joint, explains the observed behavior of each joint.

HJ01 was the only connection that failed during the heating phase. The header plate failed at the maximum temperature because of lack of resistance to the developed bending moment arising from very large rotations.

Joints EJ01, FJ03 and FJ02 failed during the cooling phase, in a mode 3 failure of the bottom bolt row (CEN, 2005b). These three joints share the same thickness of the

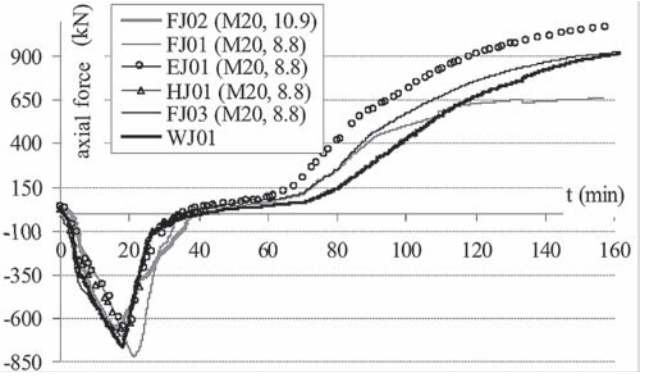

Fig. 25. Axial forces using the average temperature at the beam mid-span.

Table 9. Axial Force and the Tensile Resistance of the Bolts at Failure			
	No. of Bolts	N_{Ed}	$F_{ten,t,Rd}$
EJ01	6	1,065 kN (239 lbf)	1,330 kN (239 lbf)
FJ03	4	900 kN (202 lbf)	688 kN (154 lbf)
FJ02	4	–	890 (200 lbf)

end plate [16 mm (0.63 in.)], which prevented plastic stress redistributions within the joint and, consequently, a reduction of the applied bolt row force at the level of the bottom bolt row. As a rough approximation, based only on the axial force, Table 9 compares the applied axial force and the tensile resistance of the bolts at failure.

In Table 9, the tensile resistance of each bolt is given by

$$F_{ten,t,Rd} = \frac{0.9 k_{b,\theta} f_{ub} A_s}{\gamma_{Mfi}} \quad (2)$$

where A_s is the tensile stress area of the bolt, γ_{Mfi} is the partial safety factor for the relevant material property, for the fire situation (taken as 1.0), f_{ub} is the ultimate stress of the bolts, and $k_{b,\theta}$ is the reduction factor determined for the appropriate bolt temperature, taken as $k_{b,\theta} = 0.935$ [evaluated for a temperature of about $\theta_b = 200$ °C (392 °F), corresponding to the bolt temperature at failure]. For joint EJ01, it is clear that failure of the bolts is inevitable because of the presence of a bending moment that causes the tensile force to flow through the bottom bolts. It is noted that considering only the four bolts in tension, $F_{ten,t,Rd}$ reduce to 688 kN (155 lbf). Joints FJ03 and FJ02 also exhibit tensile failure of the bolts, more pronounced for FJ03 because of the lower grade of the bolts.

Joint FJ01, in contrast, survived the fire event in spite of a lower moment resistance because of the extra ductility provided by a thinner plate of 10 mm (0.39 in.). Joint WJ01 also survived the fire event.

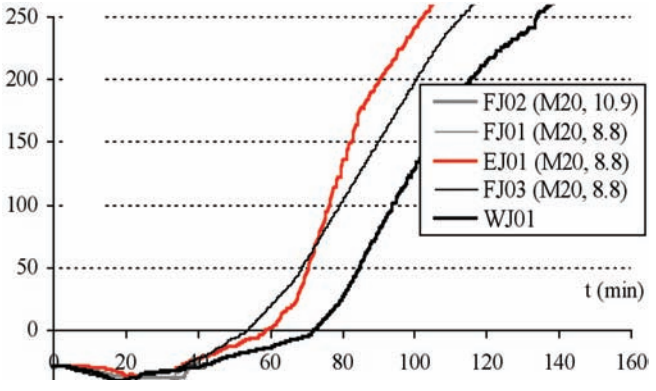

Fig. 26. Internal bending moment at the joints.

CONCLUSIONS

This paper reports on an experimental investigation on the fire behavior of a steel substructure consisting of an unprotected steel beam and connections and two fire-protected columns. Six subframes were tested whereby only the beam-to-column joints were varied. In line with current design trends, PR semi-rigid joints (at ambient temperature) were chosen, ranging from a welded configuration to several end plate typologies. In addition, for the fire loading, a relatively low applied live load ratio of 0.2 was applied (because of testing limitations).

The experimental results for the six tests show a clear influence of the joint typologies on the overall response of the subframe. The tests demonstrated the appearance of large tensile forces and the reversal of bending moment during the cooling phase, already shown numerically by the authors (Santiago et al., 2008). They also demonstrated that these forces may result in failure of the joint, as was already postulated by the authors in previous works (Simões da Silva et al., 2005).

Finally, these test results give clear indication on how to propose design guidance to avoid failure of the joints under fire loading, in the framework of the component method under fire conditions (Simões da Silva, Santiago, Vila Real and Moore, 2002). The proposed concept, for joints where the column web panel is fire protected (as was the case for these tests), is to make sure that failure of the tensile components (T-stub in tension) is controlled by the ductile end plate (mode 1) and not the bolts, both for hogging and sagging moments. This is a direct consequence of the reversal of bending moment and the subsequent M-N interaction during the cooling phase. In practical terms, this means that for most situations stronger or larger bolts should be applied in the bottom bolt row of the connection. Further details on design issues can be found in Santiago et al., 2008.

ACKNOWLEDGMENTS

Financial support from the Portuguese Ministry of Science and Higher Education (Ministério da Ciência e Ensino Superior) under contract grant POCI/ECM/55783/2004 is gratefully acknowledged.

REFERENCES

Al-Jabri, K.S. (1999), "The Behavior of Steel and Composite Beam-to-Column Connections in Fire," Doctoral Thesis, University of Sheffield, UK.

Allam, A.M., Fahad, M.K., Liu, T.C.H., Burgess, I.W., Plank, R.J. and Davies, J.M. (1999), "Effects of Restraint on the Behavior of Steel Frames in Fire," *Proc. Conference Eurosteel '99,* Praha, Czech Republic.

Bailey, C.G., Lennon, T. and Moore, D. (1999), "The Behavior of Full-Scale Steel-Framed Building Subjected to Compartment Fires," *The Structural Engineer*, Vol. 77, No. 8, pp. 15–21.

Buchanan, A.H. (2002), *Structural Design for Fire Safety*, John Wiley & Sons, England.

CEN (1992), *Eurocode 3: Design of Steel Structures—NP EN 10002-5: 1992*, European Committee for Standardization, Brussels, Belgium.

CEN (1995). *Eurocode 3: Design of Steel Structures—ENV 1993-1-2: 1995*, European Committee for Standardization, Brussels, Belgium.

CEN (2004), *Eurocode 3: Design of Steel Structures—NP EN 10025-1: 2004*, European Committee for Standardization, Brussels, Belgium.

CEN (2005a), *Eurocode 3: Design of Steel Structures—EN 1993-1-1: 2005,* European Committee for Standardization, Brussels, Belgium.

CEN (2005b), *Eurocode 3: Design of Steel Structures—EN 1993-1-8: 2005*, European Committee for Standardization, Brussels, Belgium.

CEN (2005c), *Eurocode 3: Design of Steel Structures—EN 1993-1-2: 2005*, European Committee for Standardization, Brussels, Belgium.

Lawson, R.M. (1990), "Behavior of Steel-Beam-to-Column Connections in Fire," *The Structural Engineer*, Vol. 68, No. 14, pp. 263–271.

Leston-Jones, L.C. (1997), "The Influence of Semi-Rigid Connections on the Performance of Steel Framed Structures in Fire," Doctoral Thesis, University of Sheffield, UK.

Liu, T.C.H., Fahad, M.K. and Davies, J.M. (2002), "Experimental Investigation of Behavior of Axial Restrained Steel Beams in Fire," *Journal of Constructional Steel Research*, Vol. 58, pp. 1211–1230.

Santiago, A. (2008), "Behavior of Beam-to-Column Steel Joints Under Natural Fire," Doctoral Thesis, Department of Civil Engineering, University of Coimbra, Combria, Portugal.

Santiago, A., Simões da Silva, L. and Vila Real, P. (2008), "Fire Design of Bolted Steel Beam-to-Column Joints," *Proce. International Workshop on Connections in Steel Structures: Connections VI,* Chicago, IL.

Simões da Silva, L.A.P., Santiago, A. and Vila Real, P. (2002), "A Component Model for the Behavior of Steel Joint at Elevated Temperatures," *Journal Constructional Steel Research*, Vol. 57, No. 11, pp. 1169–1195.

Simões da Silva, L., Santiago, A., Vila Real, P. and Moore, D. (2005), "Behavior of Steel Joints Under Fire Loading," *Steel and Composite Structures,* Vol. 6, pp. 485–513.

Wald, F., Simões da Silva, L., Moore, D., Lennon, T., Chladna, M., Santiago, A., Benes, M. and Borges, L. (2006a), "Experimental Behavior of a Steel Structure Under Natural Fire," *Fire Safety Journal,* Vol. 41, No. 7, pp. 509–522.

Wald, F., Chladná, M., Moore, D., Santiago, A. and Lennon, T. (2006b), "Temperature Distribution in a Full-Scale Steel Framed Building Subject to a Natural Fire," *International Journal of Steel and Composite Structures,* Vol. 6, No. 2, pp. 159–182.

Shear Behavior of A325 and A490 High-Strength Bolts in Fire and Post-Fire

LIANG YU and KARL H. FRANK

ASTM A325 and A490 bolts are widely used in bolted connections of steel structures. The strength of these heat-treated high-strength bolts at elevated temperatures is needed to determine their behavior in a fire. Understanding their response to elevated temperature is the key information required to evaluate the strength of bolted connections during a fire. The residual strength of a bolt after a fire is also important in assessing fire damage on a structure and the strategy for remediation of the structure after a fire.

Shear tests at elevated temperature were carried out on A325 and A490 bolts to investigate their change in stiffness and strength with temperature. Direct shear tests were used to determine the residual bolt strength after exposure to elevated temperatures. The shear tests were correlated with the results of hardness test of the bolts.

TEST SPECIMEN

ASTM A325 and A490 bolts, with ASTM F436 washers and ASTM A563 Grade DH nuts were tested (see Figure 1). All bolts in this test program had a nominal diameter of ⅞ in., and a length of 7 ½ in. Table 1 gives the mechanical properties of the bolts. The tensile strength listed is from the certified material test reports (CMTR). The results of room temperature shear tests on unthreaded shank of the bolt are also listed. The hardness tests reported in the CMTR and the results for the tests done on the test samples are also listed. Table 2 gives the chemical composition of the bolts as listed in the CMTR, and from a sample analyzed at an independent laboratory. Table 2 also gives the chemical composition of two sets of ISO Grade 8.8 bolts which were tested by B.R. Kirby in an earlier study (Kirby, 1995).

High-strength bolts are manufactured by annealing, cold forging of the head, rolling or cutting of the threads, and quenching and tempering to produce the required strength. Due to the variations in chemical compositions in steel rod used to make the bolts, the manufacturing tempering temperatures may be adjusted to provide final products that meet the ASTM strength and hardness requirements (ASTM A325-04; ASTM A490-04). Variations in the chemical composition and tempering process may affect the bolts behavior at elevated temperature and their residual strength after exposure to a fire. To reduce the variability of the results, all of the bolts came from the same production lot.

TEST SETUP

Shear Test at Elevated Temperature

The high-temperature test system consists of an electric furnace, stainless steel loading clevises, load frame, hydraulic ram, and data acquisition equipment. Figure 2 shows the arrangement for the elevated temperature double-shear bolt tests.

Specimen temperature was monitored by two type K thermocouples attached at both ends of the bolt. The average temperature of the readings from both thermocouples was taken as the specimen temperature. The resolution of temperature readings is ±0.1 °C (±1.8 °F). Figure 3 shows the furnace heating curve along with the ASTM standard fire curve (ASTM E119-00a). The heating curve was much slower than the standard fire test used to determine a fire rating for a product or system. The purpose of these tests was not to develop a fire rating but rather to establish the strength of the bolts when they reach a certain temperature. The average heating rate was about 2.0 °C/min (3.6 °F/min). Load was applied by hydraulic ram using a pneumatic pump to supply the hydraulic pressure when the test temperature was

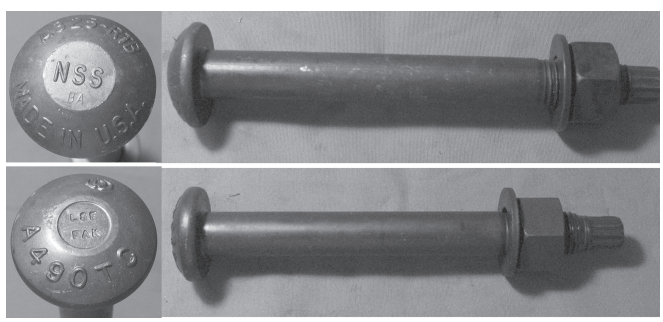

Fig. 1. A325 and A490 specimen bolts.

Liang Yu is senior engineer, Deepflex, Inc., Houston, TX.

Karl H. Frank is professor, department of civil, architectural and environmental engineering, University of Texas at Austin, Austin, TX.

Table 1. Mechanical Properties and Geometries of Tested A325 and A490 Bolts				
Item	A325		A490	
	CMTR Tensile	Shear Strength	CMTR Tensile	Shear Strength
Strength (ksi)	134.8	84.3	163.5	106.7
Hardness (HRC)	CMTR – 28~32 Test Bolts – 30		CMTR – 35 Test Bolts – 37	

Table 2. Chemical Composition of Specimen A325 and A490 Bolts												
Bolt	Data Source	Chemical Composition (wt%)										
		C	Si	Mn	P	S	Cr	Mo	Ni	B	Cu	N
ASTM A325	CMTR	0.31	0.23	0.76	0.005	0.010	–	–	–	–	–	–
	Test Sample	0.29	0.27	0.76	0.006	0.010	0.05	0.010	0.06	0.0009	0.12	0.026
ASTM A490	CMTR	0.35	0.21	0.75	0.012	0.009	1.02	0.19	0.02	–	–	–
	Test Sample	0.36	0.24	0.76	0.015	0.009	1.13	0.180	0.04	<0.0005	0.03	0.023
ISO R898 8.8	Kirby 1995 Set A	0.19	0.21	1.16	0.020	0.017	0.19	0.027	0.14	0.0051	0.22	0.0080
ISO R898 8.8	Kirby 1995 Set C	0.41	0.16	1.61	0.021	0.038	0.13	0.130	0.12	<0.0005	0.23	0.013

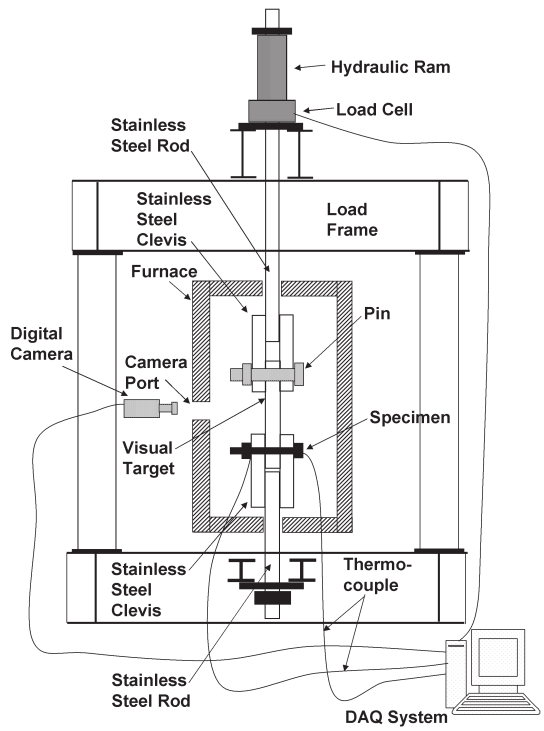

Fig. 2. Test setup for double-shear test on bolt at elevated temperature.

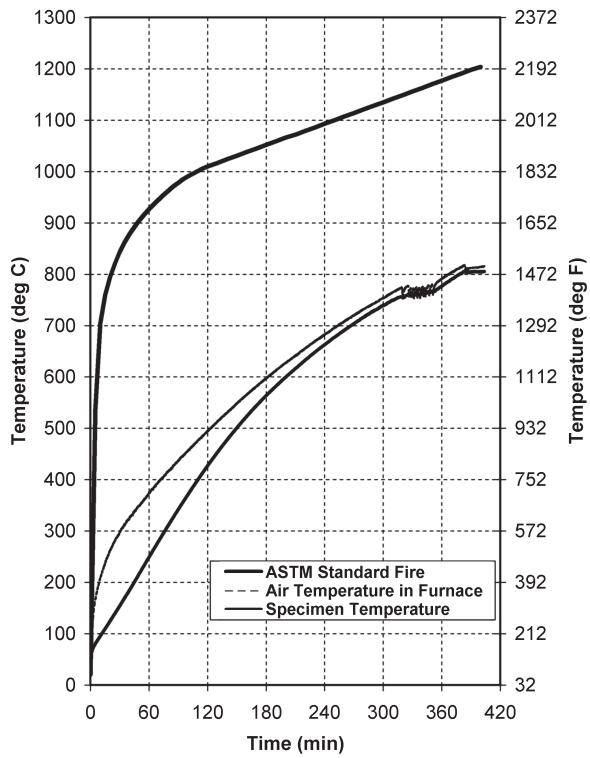

Fig. 3. Time-temperature curve of furnace.

reached. The load was measured by a 200 kip load cell with ±0.1% accuracy. Noncontact machine vision technology is used in measuring shear deformation of a specimen bolt. A 1/16-in.-diameter hole was drilled on a center loading plate to provide a visual target. A digital video camera was used to take real-time images through an observation port. Deformation was obtained by custom software. The resolution of the measured displacement was 0.005 in.

All the tests were conducted at constant temperature with quasi-static loading until failure. The test bolt was inserted through the holes into the bottom of the clevis plates and the center plate. The specimen bolt was then tightened by hand to minimize transmission of the shear force by friction. Both shear planes were in the unthreaded shank of the bolt. The specimen bolt was heated to the desired temperature level and held at the temperature to ensure uniform temperature distribution before the load was applied to the specimen. The shear load is applied by the hydraulic ram attached to the center plate by a stainless steel rod. The shear failures on both shear planes occurred simultaneously and symmetrically, which indicated the load was distributed evenly between the two shear planes. Therefore, half of the maximum load recorded in these double-shear tests by the load cell is taken as the single-shear capacity of the bolt. A minimum of two tests were performed at each temperature level for each bolt type. If the results were scattered, a third test was performed to confirm the test results.

Residual Strength Test Procedure

Both direct shear tests and hardness tests were carried out at ambient temperature to investigate residual strength of the bolts after exposure to elevated temperature. The direct shear test was performed with a single-shear fixture shown in the bottom left of Figure 4 using a test machine to apply the shear load. The hardness testing was performed on the machined and polished section of the shank of the bolt in a standard Rockwell hardness tester. The bolt segments used in both shear and hardness tests were obtained from the undeformed region of the bolts that had been tested at elevated temperature. Figure 4 shows the portion of the bolts used for direct shear test and hardness tests. The hardness test points on bolt section are also shown.

EVALUATION OF TEST RESULTS

Shear Strength at Elevated Temperature

The double-shear tests on A325 and A490 bolts were performed from 25 to 800 °C (77 to 1,470 °F) in 100 °C (180 °F) increments. Figure 5 shows load-displacement curves of A325 bolt shear tests from 25 to 700 °C (77 to 1290 °F). Due to a malfunction of the data acquisition system, the displacement data are not available for the tests performed at 800 °C (1470 °F). However, the load data were recorded properly. From 25 to 200 °C (77 to 390 °F), the initial shear stiffness of the A325 bolt is not affected by the test temperature. A slight strength increase occurs at 200 °C (390 °F), the blue brittle temperature range of steel, and the load displacement curve ends abruptly at peak load. From 400 to 700 °C (750 to 1290 °F), both the strength and stiffness of A325 bolt drops dramatically with temperature. The long unloading part on load-displacement curve reveals increased ductility of bolt at these temperatures.

Figure 6 gives the load-displacement curves of double-shear tests on A490 bolt from 33 to 800 °C (90 to 1470 °F). From 33 to 200 °C (90 to 390 °F), the strength of A490 bolt decreases slightly with temperature and reaches a minimum at 200 °C (390 °F). The strength then increases at 300 °C (570 °F). From 400 to 800 °C (750 to 1470 °F), the A490 bolt

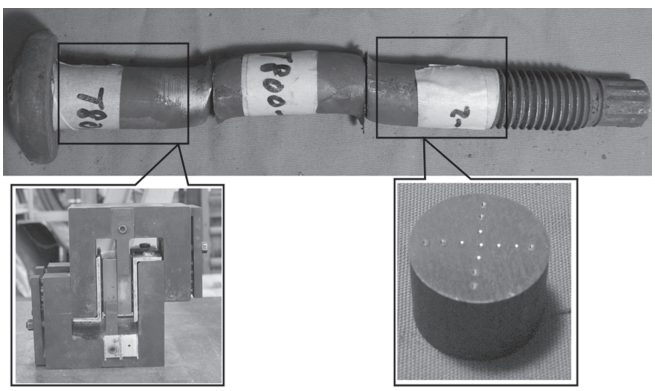

Fig. 4. Bolt segments for direct shear test and hardness test.

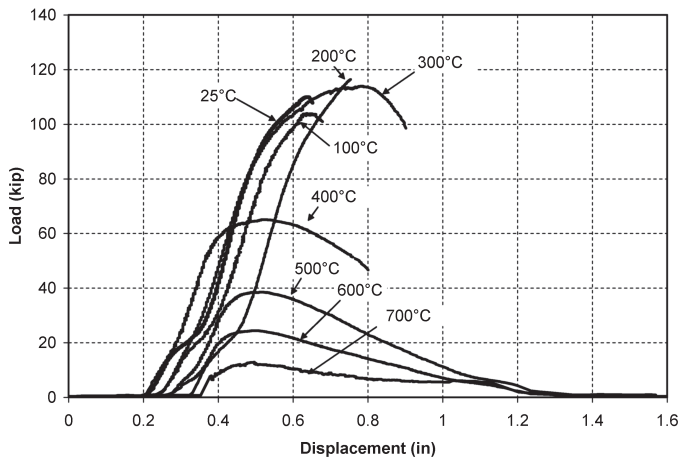

Fig. 5. Load-displacement curves of double-shear test on A325 bolt.

behaves similarly to the A325 bolt with both the strength and stiffness decreasing and the ductility increasing with increasing temperature.

Shear strengths of A325 and A490 bolts at elevated temperatures are shown in Figure 7. The shear capacity of A325 bolts changed slightly below 300 °C (570 °F) with maximum value at 200 °C (390 °F). Between 300 °C and 700 °C (570 °F and 1290 °F), shear capacity dropped dramatically with temperature. The shear capacity remains constant between 700 °C and 800 °C (1290 °F and 1470 °F). From 33 to 300 °C (90 to 570 °F), shear capacity of A490 bolt drops by about 5% at 200 °C (390 °F) first and then comes back at 300 °C (570 °F). Beyond 300 °C (570 °F), shear capacity drops almost linearly with temperature. At 400 °C (752 °F), 500 °C (932 °F), 600 °C (1110 °F) and 700 °C (1290 °F), the shear capacity drops by 17%, 40%, 65% and 85%, respectively.

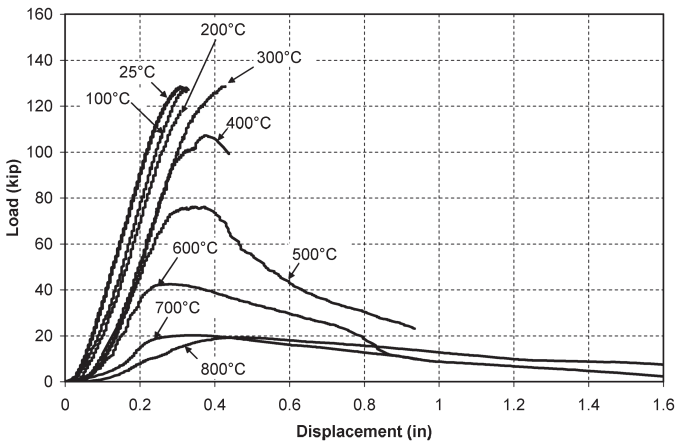

Fig. 6. Load-displacement curves of double-shear tests on A490 bolts.

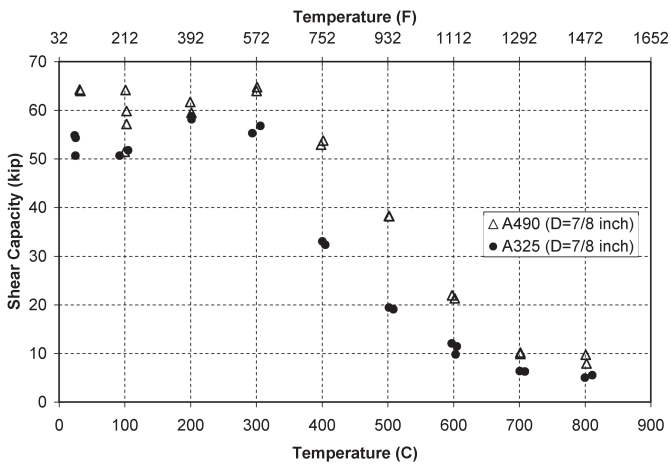

Fig. 7. Shear capacities of A325 and A490 bolts at elevated temperatures.

From 700 to 800 °C (1290 to 1470 °F), the shear capacity is essentially constant. Replicate test results are very consistent at all temperature levels for both types of bolts except for the A490 bolts tested at 100 °C (210 °F).

The shear strength relative to the room temperature capacity provides a means of developing design values at elevated temperatures. The relative shear capacity, or normalized shear capacity, is defined as the ratio of the shear capacity at elevated temperature to the shear capacity at ambient temperature. Figure 8 gives the normalized shear capacity of both types of bolts. Differences in the behavior of bolt types are evident in two temperature ranges. One is near 200 °C (390 °F), where A325 bolt has about 15% higher normalized shear capacity than A490; the other is from 300 to 700 °C (570 to 1290 °F), where the A490 bolts have significantly higher relative shear capacity than the A325 bolts.

Kirby performed a series of double-shear tests on a M20 Grade 8.8 high-strength bolt, the metric equivalent to an A325 bolt, at elevated temperature levels (Kirby, 1995). Two different lots of bolts, lot A and lot C, were tested. The chemical compositions of these two lots of bolts are given in Table 2.

Figure 9 shows the normalized shear capacity of A325, A490 and Grade 8.8 bolts. It is found that A490 bolt behaves very similarly to Grade 8.8 bolts, while A325 bolt does not. From ambient temperature to 300 °C (570 °F), A490 and Grade 8.8 bolts exhibit similar behavior. The A325 bolt shows a unique peak at 200 °C (390 °F). From 300 to 600 °C (570 to 1110 °F), the A490 bolt has a higher strength than the Grade 8.8 bolts. In the same temperature range, the A325 bolt shows significantly lower strength than the other three bolts. The difference in molybdenum contents between the bolts may be the cause of this difference in elevated temperature strength. Molybdenum can greatly increase steel

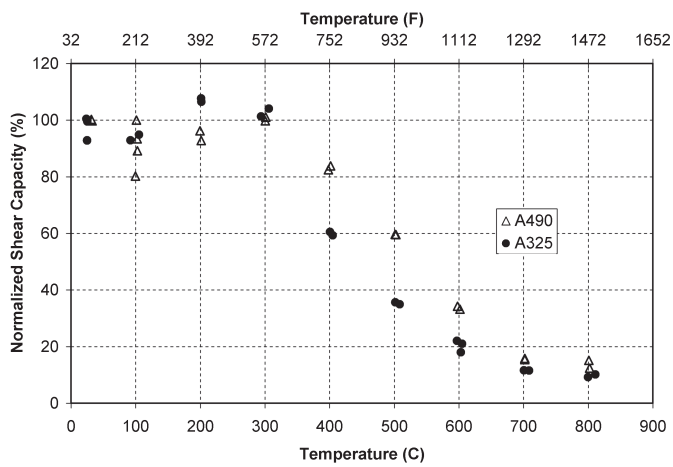

Fig. 8. Relative shear capacity of A325 and A490 bolts at elevated temperature.

strength at medium temperature range (Honeycombe, 1981; DeGarmo, 1979). The molybdenum contents of A490, Set C, Set A and A325 bolts are 0.180%, 0.130%, 0.027% and 0.010%, respectively, which corresponds to the sequence of normalized strength from high to low in the temperature range of 300 to 600 °C (570 to 1110 °F). At 700 °C and 800 °C (1290 °F and 1470 °F), the normalized shear capacity of the four groups of bolts converged to 12 to 15% of the room temperature value. Careful readers may notice that the four groups of bolts have significant differences in other alloy contents, such as carbon, manganese and boron, as well. Because those three alloy elements mainly affect the hardenability of steel but not the strength at elevated temperatures, the normalized shear strength shows no correlation with the percentage of those elements.

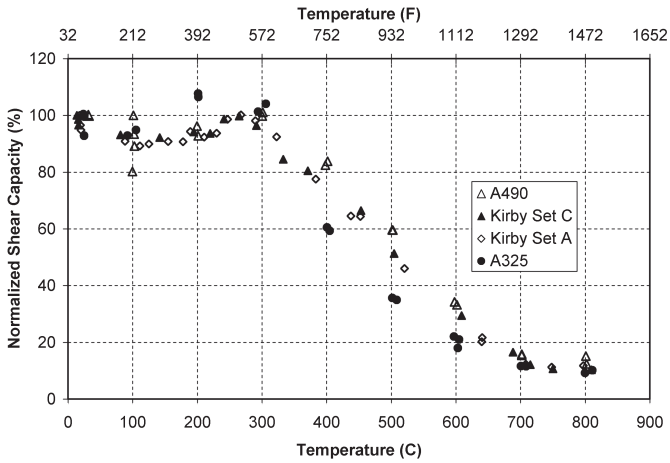

Fig. 9. Comparison of A325 and A490 high-strength bolts with Grade 8.8 M20 high-strength bolts.

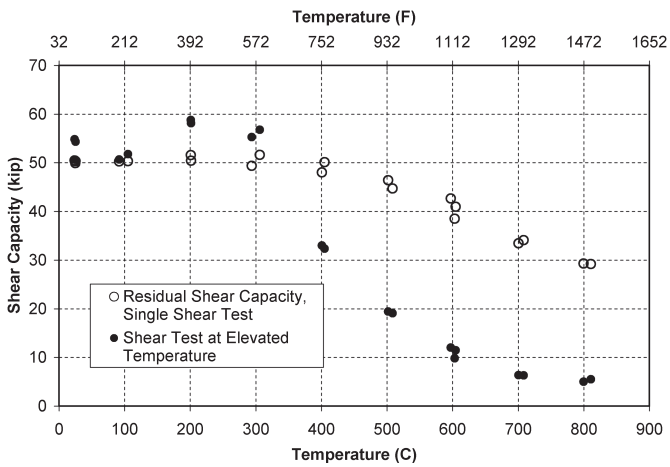

Fig. 10. Elevated temperature and residual shear capacity of A325 bolts.

Residual Shear Capacity Post-Exposure to Elevated Temperature

Figure 10 compares the residual shear capacity of A325 bolts with their shear capacity at corresponding elevated temperature levels. The tests show that if an A325 bolt is exposed to a temperature lower than 400 °C (750 °F), the bolt strength is fully recovered after cooling back to ambient temperature. A bolt exposed to a temperature higher than 400 °C (750 °F) has a lower strength after returning to ambient temperature. The A325 bolt loses strength linearly after heating to temperatures between 400 °C and 800 °C (750 °F and 1470 °F). The residual strength was about 55% of the room temperature strength after exposure to 800 °C (1470 °F). It is very interesting that the shear strength at temperatures of 200 °C and 300 °C (390 °F and 570 °F) are higher than the corresponding residual shear strength. The reason could be the changes steel microstructure in the blue brittle temperature range. This microstructure change may increase steel strength and decrease ductility (Honeycombe, 1981).

Figure 11 shows the residual shear capacity of A490 bolts along with their shear capacity at corresponding temperature levels. The A490 bolts behaved differently from A325 bolts. From ambient temperature to 300 °C (570 °F), A490 bolts had residual shear capacity close to the shear capacity at the elevated temperature, which was slightly above the initial room temperature strength. The A490 bolt showed no loss of strength after being subjected to temperature of 500 °C (930 °F). Above 500 °C (930 °F), the A490 bolt lost its strength linearly as the exposure temperature increased. The shear strength of the A490 bolts was 60% of the original room temperature strength after heating to 800 °C (1470 °F).

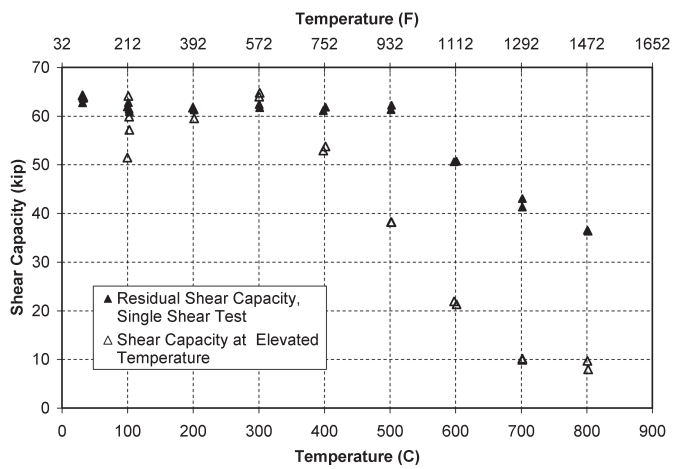

Fig. 11. Elevated temperature and residual shear capacity of A490 bolts.

Table 3. Estimated Residual Tensile Strength with Different Cooling Rate			
Estimated Tensile Strength (ksi)	Cooling Method		
	In Room Air	In Ice Water	In Furnace
Bolt #1	113	112	111
Bolt #2	105.0	–	103.7

The strength of heat-treated bolts decreased because the temperature they were exposed to was higher than the tempering temperature during manufacturing (DeGarmo, 1979). The heating of a bolt to a temperature above tempering temperature re-tempers the bolt to a lower strength level. Exposure to temperatures below the tempering temperature does not reduce the strength of the bolts. The tempering temperatures of the bolts tested in this study are estimated to be 400 °C and 500 °C (750 °F and 930 °F), respectively, for the A325 and A490 bolts.

Hardness testing of the bolts was examined as an alternative method to estimate residual strength. Hardness testing does not require special shear test fixture and is much simpler to perform. The process involves using hardness measurements to estimate the tensile strength of the fastener. The tensile strength was estimated using Table 2 and Table 3 in ASTM A370 (ASTM, 2003). The shear strength was estimated by multiplying the estimated tensile strength by 0.6 to approximate the shear strength of the fastener and then multiplying by the gross area of the bolt. The results were compared with single-shear test results.

Figures 12 and 13 show the estimated residual shear capacity of A325 and A490 bolts based upon area weighted hardness and hardness at the quarter diameter location, ½*R*, along with the results from single-shear tests. For both types of bolts, the shear capacity estimated from the hardness tests provides a very good estimate of the direct single-shear test results from ambient temperature to 600 °C (1110 °F). Estimated shear capacity was conservative, compared with shear test results, at 700 °C and 800 °C (1290 °F and 1470 °F). For both types of bolts, the hardness value at the ½*R* position, provided a good estimation of the area weighted hardness value for the whole section. Therefore, only a single set of measurements at mid-point between the center and edge of the bolt is needed to estimate the shear strength of the bolt after a fire.

The effect of duration that a bolt is exposed to elevated temperature on its residual strength was also investigated. Two A325 bolts were cut into five segments each and exposed to 600 °C (1110 °F) for different lengths of time. After being cooled to ambient temperature, hardness tests were performed. The estimated tensile strength based upon the hardness versus the length of time that it was kept at 600 °C (1110 °F) is plotted in Figure 14. It is found that an additional 330 minutes (5.5 hours) of exposure at 600 °C (1110 °F) results in an additional 10% reduction in tensile strength for these A325 bolts.

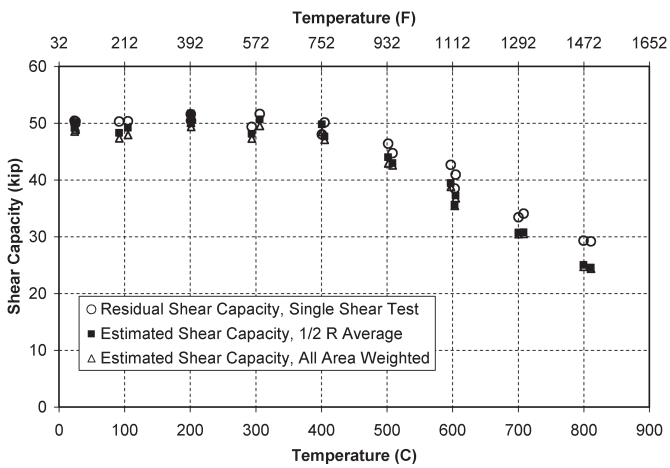

Fig. 12. Estimated residual shear capacity of A325 bolts.

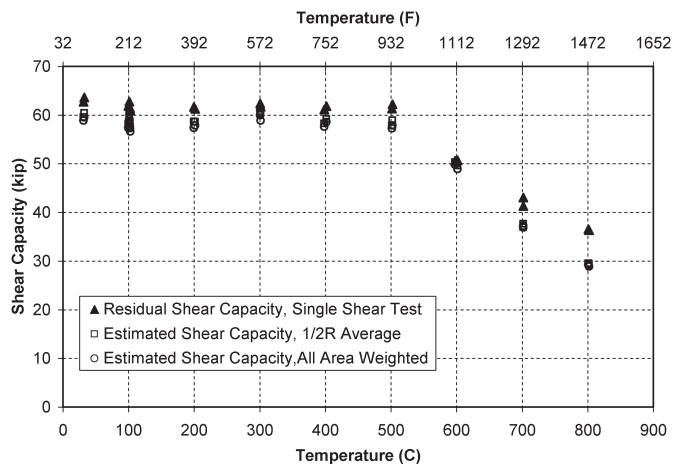

Fig. 13. Estimated residual shear capacity of A490 bolts.

Table 4. Shear Strength Reduction Factor for Tested A325 and A490 Bolts at Elevated Temperatures					
A325			**A490**		
Temperature (T_a)		Reduction Factor	Temperature (T_a)		Reduction Factor
°C	°F		°C	°F	
25	77	1.00	32	89	1.00
99	209	0.96	101	214	0.91
202	396	1.00	200	393	0.95
300	572	1.00	301	573	1.00
403	757	0.61	400	752	0.83
506	943	0.36	502	935	0.60
600	1112	0.21	600	1111	0.34
705	1301	0.12	702	1295	0.16
803	1477	0.10	801	1475	0.14

The effect of the cooling rate on the bolts residual strength was also studied. Segments from one A325 bolt were heated to 600 °C (1110 °F) for 6 hours and then cooled in room air, in ice water, and in a furnace. The time for the bolt segment temperature to reach room temperature is estimated to be 30 minutes, 5 seconds and 12 hours for these three conditions. The results in Table 3 show that the cooling rate has no effect on the residual tensile strength of A325 bolt.

CONCLUSIONS

Shear tests on ASTM A325 and A490 bolts were carried out from ambient temperature to 800 °C (1470 °F). From both types of bolts, the strength and stiffness of the bolts reduce between 300 °C and 700 °C (570 °F and 1290 °F). Table 4 summarizes the strength reduction factors from test results, which can be used to estimate the shear strength of bolted connection in a fire.

The residual strength of A325 and A490 bolts after a fire or after exposure to elevated temperature was investigated with both direct shear test and hardness test. Both types of bolts lose strength when heated above tempering temperature used in heat treatment of the bolts. The maximum strength loss for A325 and A490 bolt after exposure to 800 °C (1472 °F) are about 45% and 40%, respectively. Simple hardness test of a bolt after a fire can be used to estimate the shear strength of the bolt.

An experimental study on A325 bolt showed that the duration of exposure to elevated temperature has a limited effect on residual strength. The cooling rate has almost no effect on residual strength.

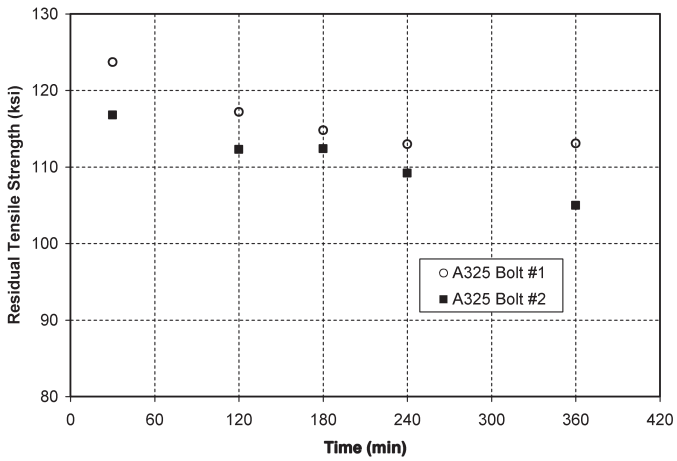

Fig. 14. Estimated residual tensile strength vs. duration of exposure to elevated temperature.

REFERENCES

ASTM (2000), *Standard Test Methods for Fire Tests of Building Construction and Materials,* ASTM E119–00a, American Society for Testing and Materials.

ASTM (2003), *Standard Test Methods and Definitions for Mechanical Testing of Steel Products,* ASTM A370–03a, American Society for Testing and Materials.

ASTM (2004a), *Standard Specification for Structural Bolts, Steel, Heat Treated, 120/105 ksi Minimum Tensile Strength,* ASTM A325-04, American Society for Testing and Materials.

ASTM (2004b), *Standard Specification for Structural Bolts, Alloy Steel, Heat Treated, 150 ksi Minimum Tensile Strength,* ASTM A490-04, American Society for Testing and Materials.

DeGarmo, Paul E. (1979), *Materials and Processes in Manufacturing*, 5th Edition, Macmillan Publishing Co., New York, NY.

Honeycombe, R.W.K. (1981), *Steels Microstructures and Properties*, Metallurgy and Materials Science Series, Edward Arnold Pub., London, UK.

Kirby, B.R. (1995), "The Behavior of High-Strength Grade 8.8 Bolts in Fire," *Journal of Construction Steel Research*, Vol. 33, pp. 3–38.

DISCUSSION

Block Shear Equations Revisited...Again

Paper by HOWARD I. EPSTEIN and LANCE J. ALEKSIEWICZ
(First Quarter, 2008)

Discussion by ROBERT G. DRIVER

The authors provide a historical account of the evolution of block shear equations in the AISC *Specification* (AISC, 2005). The main conclusion of the paper is that the 2005 *Specification* and associated commentary still do not adequately account for a number of common connection configurations, and this observation has merit. The paper cites specific cases that are addressed in the AISC *Specification* commentary and indicates that the information needs to be expanded to clarify where strength reductions are required. Although one can debate the cause and nature of the capacity reduction due to in- and out-of-plane eccentricities (and many have), it comes down largely to semantics that are overshadowed by the fact that methods for accounting for connection efficiency are approximate and that the depiction of the stress distribution in these cases as being linear is in itself an idealization of the actual stress condition in the member. It is desirable from the designer's perspective for these cases to be addressed in a simple way that gives reasonably accurate estimates of capacity, with a resulting reliability index after the resistance factor is applied that is considered acceptable to the profession. Taking a broad and pragmatic view of the block shear research in the literature and the related discussions that have ensued over the past 30 years, it seems clear that the effects of load eccentricity can be addressed effectively by simple factors that are, in essence, equivalent stress factors. This discussion paper addresses two related issues arising from the original paper: (1) the format of the block shear equation itself and (2) the treatment of Tees connected by their flanges only.

It was noted by the authors of the paper that the introduction of the factor U_{bs} to the 2005 AISC block shear equations (using $U_{bs} = 0.5$) results in a least-squares trend line for test-to-predicted ratios (professional factors) of the strength of angles connected through one leg (Figure 3 of the paper) that shows a "marked improvement" over the analogous trend line generated using the 1999 *Specification* equations. What was not highlighted, with respect to this figure, however, is the gross conservatism of the predictions based on the 2005 *Specification* and the associated degree of scatter. For angles and stem-connected Tees in particular, Driver, Grondin and Kulak (2006) determined that the mean test-to-predicted ratio increased from 1.03 to 1.25 when the 1999 AISC *Specification* was replaced with the 2005 edition (using $U_{bs} = 0.5$); this is similar to the results depicted in Figure 3 for the angle tests of Epstein alone (Epstein, 1992). For interpreting whether or not this increase actually represents an improvement, it needs to be emphasized that test-to-predicted ratios greater than 1.0 are not superior to those less than 1.0. (It is the application of load and resistance factors that establish the "safety" of the method.) The measures of primary importance are the proximity of the mean ratio to 1.0, indicating how accurate the model is on average, and the magnitude of the coefficient of variation of the individual ratios, which is a measure of consistency of the accuracy of the design equation over the range of tests considered. These two parameters, when taken together, tend to indicate whether the model reflects the actual behavior sufficiently well. Making use of these principles, observations (Kulak and Grondin, 2001) of highly inconsistent results obtained using existing methods provided the impetus for the development of the unified block shear equation that has been shown to provide improved and more consistent strength predictions for a variety of connection types (Driver et al., 2006).

With regard to the specific case of Tees, the authors are quite correct that the equivalent stress factor recommended by Driver et al. (2006) applies only to stem-connected Tees. However, the unified equation has also been shown (Cai and Driver, 2008) to provide excellent results for flange-connected Tees failing along the alternate block shear path observed by Epstein and Stamberg (2002), although it is acknowledged that these results were not available to the authors of the paper when they prepared their manuscript. Using the test results of Epstein and Stamberg (2002), the

Robert G. Driver is professor, department of civil and environmental engineering, University of Alberta, Edmonton, Alberta, Canada.

unified equation, with no mean stress reduction due to load eccentricity (i.e., equivalent stress factor equal to 1.0), gives a mean test-to-predicted ratio of 1.05 with a coefficient of variation of 0.09, and, using the current resistance factor in the AISC *Specification* (0.75), the reliability index for this connection type is 4.2 (Cai and Driver, 2008). Although the authors have stated that the equivalent stress factor of 0.9 that has been recommended for stem-connected Tees may not provide a large enough reduction if it were applied also to flange-connected Tees, in fact no reduction is required for this case. The cross-sectional shape of the Tee results in an out-of-plane eccentricity of the load with respect to the block that, although indisputably present, is typically relatively small and does not affect the capacity of the member to a degree that would warrant a reduction of the strength for design. However, for some connection configurations where eccentricities are present, reductions are indeed warranted, and recommendations have been made for several common cases (Driver et al., 2006).

REFERENCES

AISC. (2005), *Specification for Structural Steel Buildings,* American Institute of Steel Construction, Chicago, IL.

Cai, Q. and Driver, R.G. (2008), "Performance of the Unified Block Shear Equation for Atypical Failure Paths," *6th International Workshop on Connections in Steel Structures*, Chicago, IL.

Driver, R.G., Grondin, G.Y. and Kulak, G.L. (2006), "Unified Block Shear Equation for Achieving Consistent Reliability," *Journal of Constructional Steel Research*, Vol. 62, No. 3, pp. 210–222.

Epstein, H. (1992), "An Experimental Study of Block Shear Failure of Angles in Tension," *Engineering Journal*, American Institute of Steel Construction, Vol. 29, Second Quarter, pp. 75–84.

Epstein, H.I. and Stamberg, H. (2002), "Block Shear and Net Section Capacities of Structural Tees in Tension: Test Results and Code Implications," *Engineering Journal*, American Institute of Steel Construction, Vol. 39, Fourth Quarter, pp. 228–239.

Kulak, G.L. and Grondin, G.Y. (2001), "AISC LRFD Rules for Block Shear in Bolted Connections—A Review." *Engineering Journal*, American Institute of Steel Construction, Vol. 38, Fourth Quarter, pp. 199–203.

CLOSURE

Block Shear Equations Revisited...Again

Paper by HOWARD I. EPSTEIN and LANCE J. ALEKSIEWICZ
(First Quarter, 2008)

Closure by HOWARD I. EPSTEIN and LANCE J. ALEKSIEWICZ

The primary conclusion of the authors' paper was the need for more cases to be included for the new block shear reduction factor (due to eccentricity), U_{bs}, less than 1.0. Of the cases suggested, angles connected by one leg are the most critical due to this common way of connecting angles. The discussion by Prof. Driver indicates that there is "gross conservatism" built into the 2005 AISC *Specification* for this case. The authors disagree. Prof. Driver's recent co-authored paper (Driver et. al., 2006) base this "gross conservatism" conclusion on a small fraction of the tests that were conducted at the University of Connecticut (Epstein, 1992) by not considering 12 of the 15 block shear failures found due to the stagger in those 12 connections. But, as already pointed out in the author's paper, "Stagger…was shown not to have an appreciable effect on capacity." Out-of-plane eccentricity is a significant factor in reduced capacity for block shear. This was also shown for flange connected tees.

The case of flange connected tees was extensively investigated at the University of Connecticut (Epstein and Stamberg, 2002). The discusser states that "…no reduction is required for this case" due to relatively small out-of-plane eccentricity. The authors disagree. The "shear lag" factor, $U = 1 - x/L$, is a strong indicator of out-of-plane eccentricity. There are many potential flange-connected Tees where U is calculated to be 0.7 or less. The discusser also indicated that the test results for flange-connected Tees of Epstein and Stamberg (2002) show no need for including an U_{bs} factor less than 1.0, and he calculated ratios and coefficients to back his point. The authors, however, would like to point out that the tests for Tees varied from very little to significant out-of-plane eccentricities, and there was a strong correlation between the $U = 1 - x/L$ factor and the need for a U_{bs} factor significantly less than 1.0.

The authors thank Prof. Driver for his discussion. From our mutual writings, it is clear that we agree that some "tweaking" of the AISC *Specification* for block shear is still very much warranted. It remains the author's opinion that "… either the definition of U_{bs} must change or the figures in the (AISC) commentary need to include more cases where U_{bs} is not equal to 1.0. As a minimum, two gage lines in an angle as well as Tees connected by their flanges and, probably, W sections connected by their flanges should be added to the cases in Figure 5b."

Howard I. Epstein is professor, department of civil and environmental engineering, University of Connecticut, Storrs, CT.

Lance J. Aleksiewicz is structural engineer, Odeh Engineers, Inc., North Providence, RI.

Current Steel Structures Research

REIDAR BJORHOVDE

As should be expected, the ultimate goal of much structural engineering research is the eventual incorporation of the key findings into design codes and related documents. The procedures for accomplishing such aims vary a great deal from country to country and within economical or geographical regions. Further, legal needs may override some potential criteria, as expressed by various code authorities. The interactions and complexities of the American system are legion, between the requirements for steel-framed buildings (AISC and AISI), the loading criteria (ASCE 7) and the overall legal framework of the building code (IBC, through ICC). Similar procedures are used in Canada, Australia, the European Union and its member countries, and many other areas. The combined complexity of the specifications, standards and codes is such that researchers ought to be intimately familiar with all of the needs that are expressed through such documents.

Aiming at improving structural efficiency, economy and above all performance for all forms of service requirements, a number of current studies are investigating novel applications of steel and composite elements and systems. Applied to buildings and bridges alike, some of the recent examinations extend well-known analysis and design concepts to uses of high-strength steel and composite members with high-strength concrete. Research work in China has developed testing and analytical procedures for cast steel connections, and design criteria have been developed through significant applications for traditional forms of steel construction such as long-span trusses. Further, structural ductility and fracture toughness are assessed through realistic and practical procedures, recognizing actual rather than theoretical needs.

Seismic considerations continue to be critical for many areas of the world, and a major effort in France is examining the behavior and strength of certain composite end plate connections. Including tests as well as extensive analytical evaluations, performance data are used in conjunction with the development of suitable models. The same research team is also developing innovative solutions for beam connections in short- and medium-span composite bridge structures. Two ongoing studies in Singapore address the use of very high strength concrete and steel in composite columns for high-rise construction, and a novel form of sandwich construction has been developed that makes use of a new type of shear connector. A recent project in the United States has examined the performance of slip-critical connections with fillers, an important application for many types of construction, especially when very heavy rolled shapes are to be utilized.

References are provided throughout the paper, whenever such are available in the public domain. However, much of the work is still in progress, and reports or publications have not yet been prepared for public dissemination.

Reidar Bjorhovde is the Research Editor of the AISC *Engineering Journal*.

STRUCTURAL BEHAVIOR AND STRENGTH UNDER SEISMIC LOADS

Static and Seismic Behavior of Steel and Composite Bolted End-Plate Beam-to-Column Connections: This project has been conducted at the Institut National des Sciences Appliquées (INSA) in Rennes, France, with Professor Alain Lachal as the director. Financial support is provided by the French Ministry for Infrastructure and Transport through the Research Management Program.

Focusing on the moment-rotation behavior and the ductility and energy absorption capacity of the connections, full-scale tests and three-dimensional finite element analysis have been conducted (Lachal et al., 2008). Figure 1 illustrates the test setup for the two- and three-dimensional specimens. Special attention has been paid to the stress and strain data for the web panels of the connections, as well as the concrete slab in the vicinity of the column and especially the part of the slab that is strengthened by the haunches. The test loading procedure was done in accordance with the protocol of the European Convention for Constructional Steelwork (ECCS, 1986).

It has been determined that the nonuniform shear stress distribution in the column panel zone that was exhibited by the tests is confirmed by the theoretical analysis. Further, the haunch appears to provide a significantly improved cyclic performance of the connection, with a plastic energy absorption that is double that of a nonhaunch connection. The researchers also have concluded that there is no risk of low-cycle fatigue fracture of the weld between the end plate and the beam flanges. The stiffening effect of the composite slab increases the positive moment capacity by 60% in comparison with a nonhaunch connection; it also prevents flange buckling. On the other hand, for negative bending the presence of the composite slab only increases the moment

capacity by about 30%, and it offers no reinforcing effect for the beam flanges.

Of significant interest for design considerations, the results show that the current Eurocode 3 (CEN, 2005a) criteria underestimate the strength and stiffness contributions of the column panel zone, especially when doubler plates that are thicker than the column web are used. In addition, the analytical evaluations demonstrate the "non-negligible" (Lachal et al., 2006) effects of tension stiffening and the use of preloaded bolts.

BEHAVIOR AND STRENGTH OF CONNECTIONS

Behavior of Slip-Critical Connections with Fillers: This is a project that has been conducted at the University of Illinois at Urbana-Champaign, with Professor Jerome F. Hajjar as the director. The project was sponsored by the American Institute of Steel Construction, W&W Steel Corporation and the University of Illinois, with in-kind support provided by Lohr Structural Fasteners and the University of Cincinnati.

Filler plates of various thicknesses are common in bolted connections when structural members of different depths are used. Lacking performance data for connections with very heavy shapes and slip-critical joints, a total of 16 full-scale tests of column splices were conducted to examine the slip and strength characteristics of connections with oversize holes. One of the tests used standard size holes, to establish a set of baseline data.

All of the test specimens used W14×730 stub column shapes; these were connected to W14×159, W14×455 and W14×730 shapes with 2-in. splice plates in addition to fillers (where necessary) of thicknesses from 1⅝ in. to 3¾ in. The filler configurations varied from undeveloped to partially developed and fully developed. Single-ply and two-ply fillers were used; the latter had filler thicknesses of 3½ and ¼ in. Some fillers were welded. Finally, the specimens were fabricated with turn-of-nut bolts or tension-control bolts.

Figure 2 shows one of the test specimens after failure, first by connection slip and then bolt shear fracture. This particular specimen had oversize holes and 1⅝ in. fillers. The researchers note that all of the test connections exhibited high resistance to slip, with only two of the cases falling below the predicted loads. Assessing these results along with data provided by other investigations, as reported in the literature, it is clear that the slip strength is reduced by the presence of undeveloped fillers, and this is independent of filler thickness and hole size. The slip strength reduction is particularly observed for connections with multi-ply fillers.

As expected, the bolt shear strength was much larger than the slip value, but the connection strength was clearly affected by the presence of any filler plates. The shear strength is initially reduced by the presence of thin fillers; for thicker fillers the strength is increased. Design requirements have been proposed to take all of these effects into account for compression splices.

Application of Connections Using Cast Structural Steel Elements: This project has been conducted at Tongji University in Shanghai, China, with Professor Yi-Yi Chen as the director. Support has been provided by the Tongji University through its research program.

The study reflects increasing attention to the use of cast steel elements in Chinese construction, many of whose

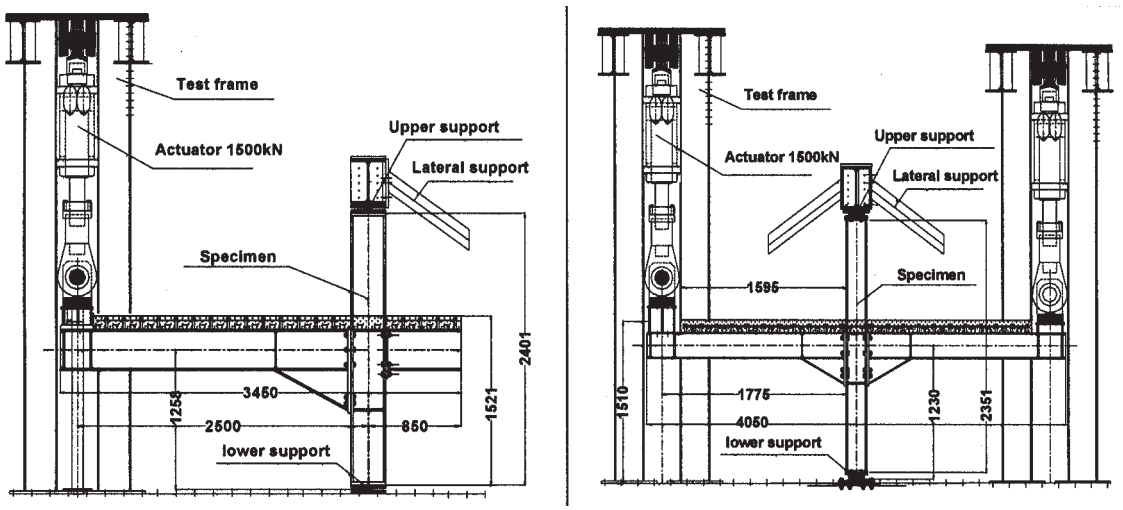

(a) Two-dimensional test (b) Three-dimensional test

Fig. 1. Connection test specimens. (Courtesy of Professor Alain Lachal)

structures and connections tend to be very complex and not easily designed in accordance with current standards. A recent (2008) addition to the family of codes aims at facilitating the use of cast steel, but much work remains to be done (Chen et al., 2008).

Using three-dimensional finite element analysis and full-scale tests of cast connections for specific structures, the researchers have developed a practical methodology for these types of connections. One of the key difficulties with the use of cast steel has been the lack of reliable material standards, but that is now being overcome. For example, the recently published Chinese standard focuses on two grades of weldable cast steel, with yield stress values from 200 to 275 MPa and tensile strength values from 400 to 485 MPa (Chen et al., 2008). The properties are comparable to those of European cast steels, which have yield stresses between 240 and 300 MPa and tensile strengths from 450 to 650 MPa (EN, 2005b). The researchers observe that full plasticity criteria should not be used for the design of these types of connections. Rather, partial plasticity may be feasible, although the favored approach is elastic analysis (allowable stress design) accompanied by physical testing. The tests that have been conducted aimed in part at confirming these considerations, which are clearly conservative choices.

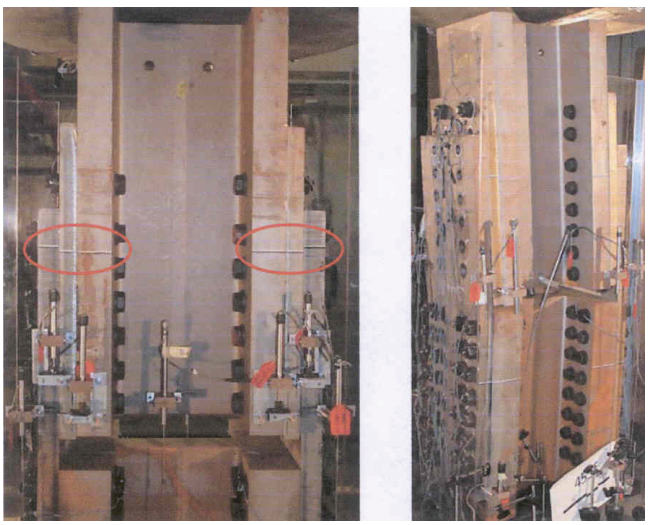

Fig. 2. Testing of heavy column splice with filler plates. (Courtesy of Professor J. F. Hajjar)

Several full-scale tests for connections in specific structures have been performed by the researchers. The details of the test specimens were determined following extensive three-dimensional finite element analyses. For example, Figure 3 shows the Laoshan Velodrome that was built for the 2008 Olympic Games, along with the structural details of the connection and the test setup.

Another example is shown in Figure 4, where the bottom chord connection to the pair of web members in a so-called beam-string truss was chosen for physical testing. The structure uses a pair of inclined (out-of-plane) trusses, connected to the single bottom chord by inclined verticals. It is noted that in addition to the cast steel part of the connection, the bottom chord and the inclined verticals are attached to the tubular elements of the casting by threads inside the tubes.

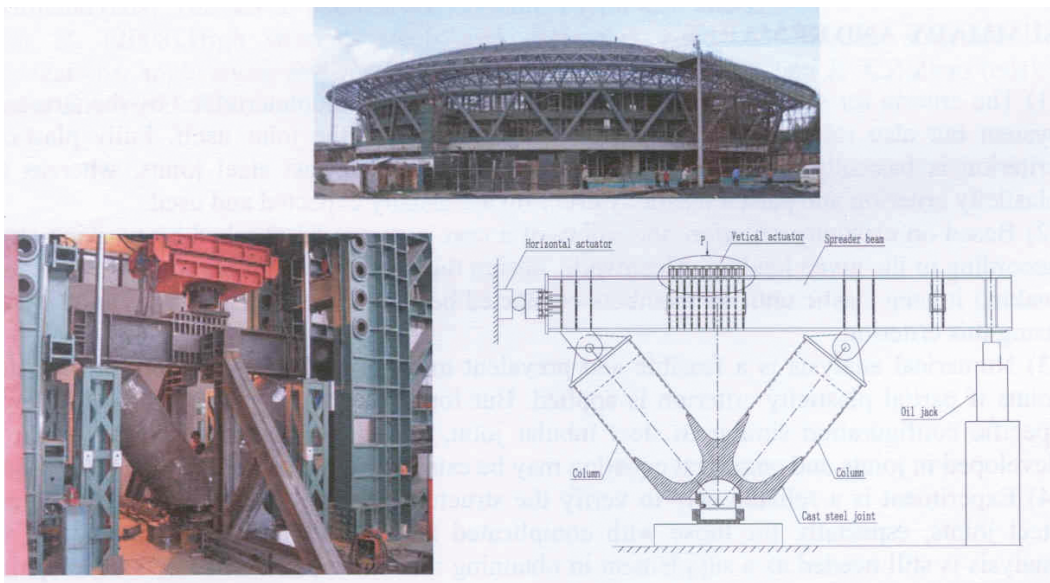

Fig. 3. Laoshan Velodrome structure and cast steel detail with test setup. (Courtesy of Professor Y.-Y. Chen)

The good correlation between test and theory for two of the critical locations within the connection is illustrated in Figure 5.

Significant additional tests and analyses have been conducted, including for more complex connection configurations. Detailed design recommendations will be forthcoming.

COMPOSITE CONSTRUCTION

Design of Composite Steel-Concrete Systems for Multi-Story Building Construction: This project is a major, long-term study being conducted at the National University of Singapore with Professor J. Y. Richard Liew as the director. Support has been provided by the National University of Singapore through its research program.

The project addresses composite member, connection and framing system issues in great detail, in addition to the performance of composite structural systems under fire and blast conditions (Liew, 2008). The strength and behavior of unique types of composite columns is of particular interest.

High-rise construction in Singapore uses composite framing systems extensively and with great innovation. The

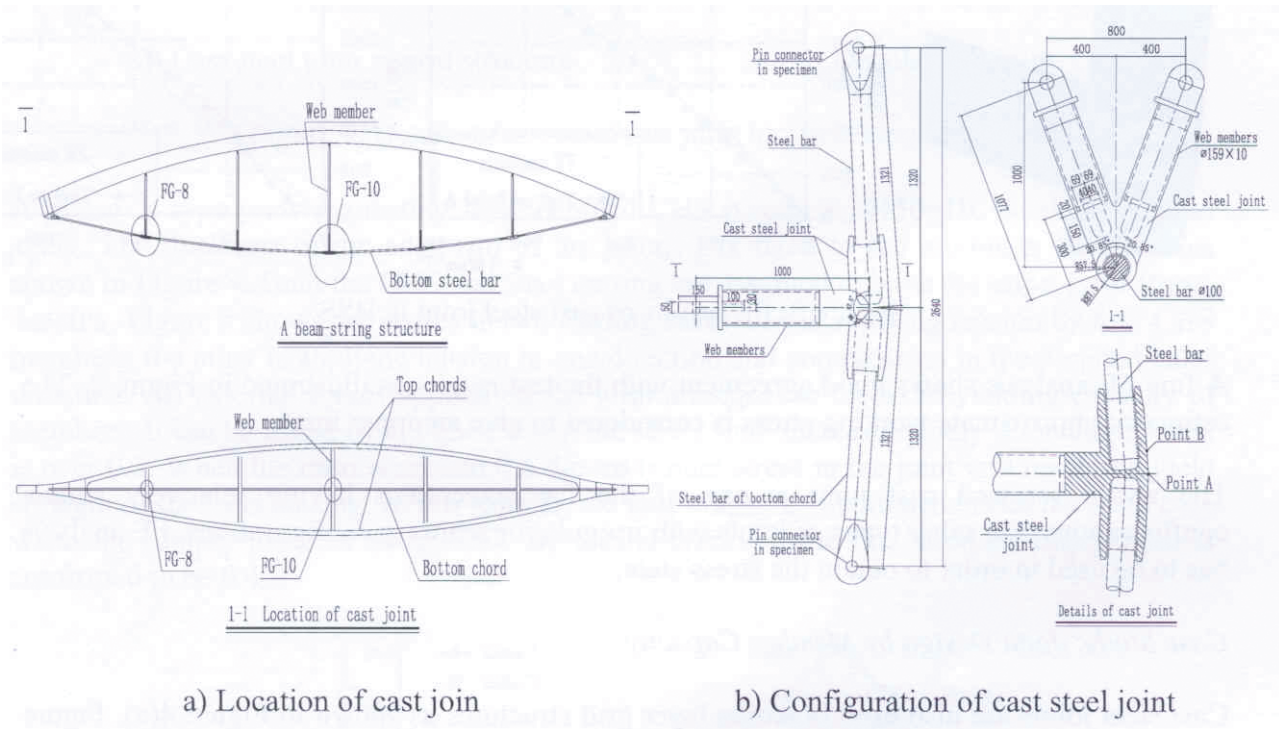

Fig. 4. Beam-string truss in elevation and plan, along with cast steel connection detail. (Courtesy of Professor Y.-Y. Chen)

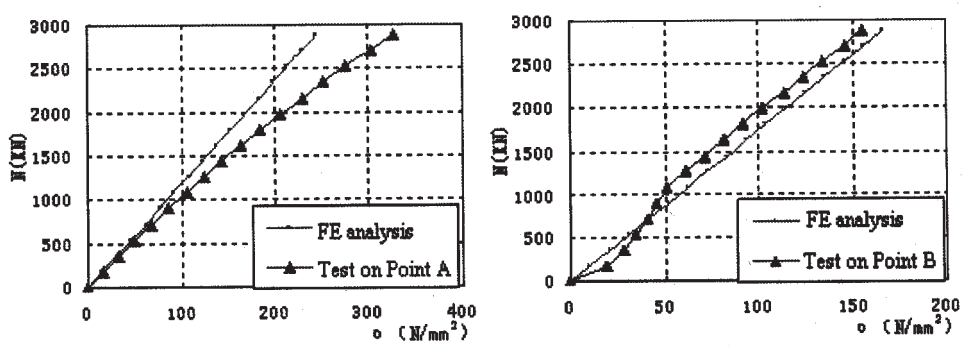

Fig. 5. Comparison of measured and computed stresses at points A and B (see Fig. 4). (Courtesy of Professor Y.-Y. Chen)

composite columns have enabled architects and designers to develop structures with larger usable floor areas and higher lateral load resistance. As shown in Figure 6a, concrete-filled round HSS was used to significant advantage for certain low- and mid-rise buildings, although the large wall thickness that was needed led to high construction cost. Further, the limitations for the sizes of the available steel cross-sections restricted the uses in high-rise frames.

The issues related to composite columns have effectively been resolved through the use of columns with either high-strength steel cores, as shown in Figure 6b, and especially with the use of an internal round HSS filled with ultra-high-performance concrete (UPHC), as shown in Figure 6c. Although the strength and fire resistance of the steel-core column in Figure 6b are high, the high-strength steel is expensive. The researchers observe that the tube-in-tube solution is a significant improvement in all respects, since normal strength concrete (5 to 7 ksi strength) may be used for the filling between the outer and inner walls of the two tubes. The UPHC is only used as the filling for the interior tube; the strength of this concrete material may be as high as 25 ksi (Liew, 2008).

This research work is continuing, including studies of the connections between the inner and outer tubular members, using various forms of shear keys. The use of shear keys between the concrete slab and the tube-in-tube column has produced an effective "slim floor" design that does not require additional fire protection. Primary analyses have demonstrated potential cost savings of the tube-in-tube column of 20 to 50% when compared to the solid steel core case.

Structural Performance of Steel-Concrete-Steel Sandwich Composite Structures: This is a major study being conducted at the National University of Singapore with Professor J. Y. Richard Liew as the director. The project has been sponsored by the Maritime and Port Authority of Singapore, Keppel Offshore & Marine Ltd. and the National University of Singapore.

As a low-weight, high-performance structural system with especially high resistance to impact and blast, steel-concrete-steel sandwich elements have been used for a number of applications since the early 1990s (Liew and Sohel, 2008). The original applications were bridge decks in long- and medium-span structures, although these solutions had a number of drawbacks in the form of bonding failure between the steel and internal concrete parts. Improved composite response through better shear connection features have made the sandwich elements very suitable for offshore and ship structures as well as caissons, core walls and submerged tunnel construction.

The key feature of a successful steel-concrete-steel sandwich element is the shear connectors that enable the components to function as an integral unit, along with the use of lightweight concrete. Traditional headed stud shear connectors may be used, and solutions such as the "bi-steel" sandwich panel have offered usable solutions. However, the difficulties with these two forms of construction are very significant insofar as constructability is concerned: it is simply very difficult to build and ensure satisfactory shear transfer between the steel and the concrete, and especially to pour the concrete itself. Prefabrication is a possible solution, but this offers practical problems due to the weight and physical sizes of the elements.

The novel and ingenious solution offered by the researchers is the development of a new form of shear connector, the J-hook connector, as illustrated in Figure 7. This is a patented detail and is essential to the construction and service performance of the sandwich elements. Extensive physical testing has been done, to examine the performance of the connectors and the sandwich system under tensile loading (perpendicular to the steel plate and longitudinal to the connectors), as well as bending and impact tests for

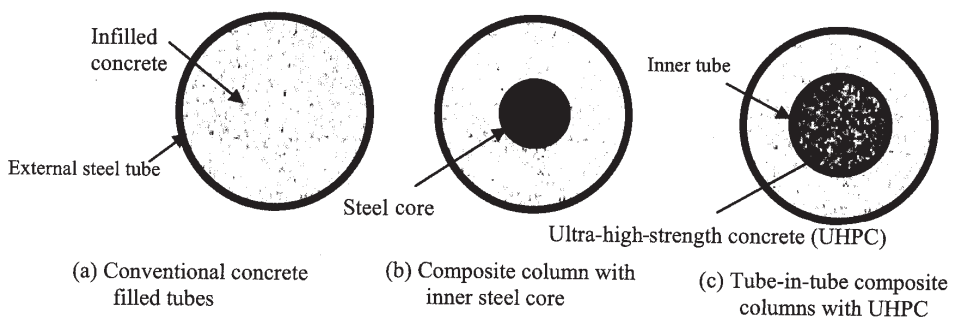

Fig. 6. Various tubular composite column cross-sections. (Courtesy of Professor J. Y. Richard Liew)

the sandwich elements. It has been found that the concrete cracking that was a serious difficulty for the original concept has been reduced significantly, and the blast and impact resistance is very high. The impact tests in particular offer very interesting results.

The research and development work will continue, with anticipated applications for numerous structures associated with maritime construction, improved bridge and roadway elements, and potential shear wall structures in buildings. Ductility issues will continue to be addressed, especially as it appears that adding steel or other fibers to the concrete mix will improve the overall response.

PERFORMANCE OF BRIDGE STRUCTURES

Innovative Solutions for Beam Connections in Small and Medium Span Composite Bridges: The project is conducted at the Institut National des Sciences Appliquées (INSA) in Rennes, France, with Professor Alain Lachal as the director. It has been funded by the Ministry for Infrastructure and Transport of France through the Research Management Program.

This is a longer-term project aimed at improving the economies of short- and medium-span bridges. Bridge designers in France have commonly used various forms of bolted end plates, and the study examines such connections as well as plates with stud shear connectors that are embedded into the concrete, and connections that are fully embedded into the concrete. Full-scale tests have been conducted, looking at the performance of the connections fatigue loading, followed by monotonic loading to failure. The researchers feel that this establishes a complete database that will be useful in further studies.

Extensive three-dimensional finite element analyses are being performed to correlate the analysis with the full-scale tests. The aim is to provide a complete analytical design method for the connections that are being tested, with potential extension to additional connections and other bridge types.

REFERENCES

Chen, Y.-Y., Zhao, X.-Z. and Tong, L.-W. (2008), "Research and Application of Connections of Structural Steel Casting," in *Innovations in Structural Steel,* Regency Steel Asia International Symposium, December 1, 2008, S.-P. Chiew, Editor, Nanyang Technological University, Singapore, pp. 88–102.

CEN (Comité Européen de Normalisation) (2005a), *Eurocode 3—Design of Steel Structures—EN 1993-1*, CEN, Brussels, Belgium.

CEN (Comité Européen de Normalisation) (2005b), *Steel Castings for General Engineering Uses—EN 10293*, CEN, Brussels, Belgium.

European Convention for Constructional Steelwork (ECCS) (1986), *Recommended Testing Procedures for Assessing the Behaviour of Structural Elements under Cyclic Loads*, ECCS Task Committee 1, Technical Working Group 1.3, Seismic Design, Report No. 45.

Lachal, A., Aribert, J.-M. and Loho, G. (2006), "Analytical and Experimental Investigations of Bolted Haunched Beam-to-Column Joints with a View of Seismic Design," *Advanced Steel Construction*, Vol. 2, June, pp. 135–160.

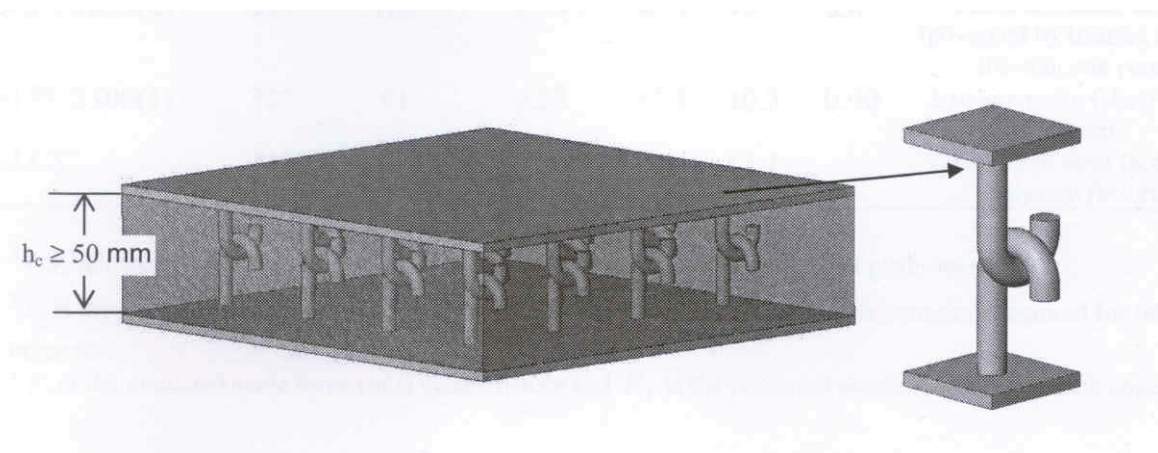

Fig. 7. Steel-concrete-steel sandwich element with J-hook shear connectors. (Courtesy of Professor J. Y. Richard Liew)

Liew, J. Y. Richard (2008), "Design of Steel-Concrete Composite Systems for Multi-Storey Building Construction," in *Innovations in Structural Steel*, Regency Steel Asia International Symposium, December 1, 2008, S.-P. Chiew, Editor, Nanyang Technological University, Singapore, pp. 124–191.

Liew., J. Y. Richard and Sohel, K. M. A. (2008), "Structural Performance of Steel-Concrete-Steel Sandwich Composite Structures," in *Innovative Design of Steel Structures*, Second International Symposium, December 5, 2008, Ben Young, Editor, The University of Hong Kong, Hong Kong, China, pp. 73–100.

ACKNOWLEDGMENTS

Special thanks are due the following members of the International Structural Steel Research Advisors (ISSRA) who provided input to this paper:

Andre Colson, National Federation for Public Work (FNTP), Paris, France

J. Y. Richard Liew, National University of Singapore, Singapore

G.-Q. Li, Tongji University, Shanghai, China

Additional assistance has been provided by Jerome F. Hajjar, University of Illinois, Urbana, Illinois; Alain Lachal, INSA-Rennes, Rennes, France; Y.-Y. Chen, Tongji University, Shanghai, China; S.-P. Chiew, Nanyang Technological University, Singapore; Ben Young, The University of Hong Kong, China; and Thomas Schlafly, AISC's Director of Research.

Suggested Readings from Other Publishers

The following abstracts have been prepared by Reidar Bjorhovde, Research Editor of the AISC *Engineering Journal*

From Volume 64, Number 7–8, 2008 of the *Journal of Constructional Steel Research* published by Elsevier, Ltd.:

Survivability of Steel Frame Structures Subject to Blast and Fire
J. Y. Richard Liew

A numerical model that facilitates frame analysis for a structure that has been damaged by blast and subsequently is subjected to fire is developed. The approach captures the details of the behavior of the frame members, including stability effects in the presence of the high strain rates associated with the blast. Fire-blast interaction diagrams are presented—these are used to determine the fire resistance of the blast-damaged members. Following the complete analysis of a multi-story frame, to allow the quantification of the complex interaction between fire and blast, it is shown that the frame has low fire resistance in the aftermath of the blast.

From Volume 64, Number 10, 2008 of the *Journal of Constructional Steel Research* published by Elsevier, Ltd.:

New Method of Inelastic Buckling Analysis for Steel Frames
Hoon Yoo and Dong-Ho Choi

The inelastic method of analysis that is presented is based on the concepts of modified bifurcation stability theory, using the tangent modulus approach along with the column curves and the interaction equation for beam columns. The results show that the proposed inelastic evaluation gives a correct assessment of the critical load as well as the stability limit states for the frame.

From Volume 64, Number 12, 2008 of the *Journal of Constructional Steel Research,* published by Elsevier, Ltd.:

Lateral Buckling of Web-Tapered I-Beams: A New Theory
Zhang Lei and Tong Geng-Shu

A linear analysis is first conducted to take into account the effects of the tapering of the members, ensuring deformation compatibility between the flanges and the tapered web. Following a total potential energy analysis, it is found that these results compare favorably with those of a finite element approach. Further, the study shows that the proposed approach gives results that are significantly better than those of a traditional prismatic beam element model. In fact, it is shown that the equivalent method of using prismatic beam elements may give unreliable buckling loads for tapered beams.

From Volume 4, Number 4, 2008 of *Advanced Steel Construction:*

Behavior and Design of Laterally Braced Inelastic Compression Members
Eric M. Lui and Ajit C. Khanse

A pseudo-load method of inelastic analysis is used to trace the load-deflection behavior of the member up to and including the buckling limit state. The compression member in question is pinned at both ends and braced at an intermediate point. The brace is modeled as an elastic spring, although the member itself may behave inelastically during the loading procedure. It has been found that the so-called fully braced condition is rarely developed, and the actual strength may therefore fall below that predicted by the design code. Design equations for the strength and stiffness of the brace are proposed—these are based on the concept that the compression member will develop at least 90% of the code-specified column strength.

The following abstracts have been prepared by AISC staff:

From the October 2008 (Volume 86, No. 19) issue of *The Structural Engineer*, published by the Institution of Structural Engineers.

Design for Robustness of Connections to Concrete Filled Tubular Columns in Fire
Summer Ding

Concrete filled tubular (CFT) columns were found to experience failure in the joint region under fire conditions. An extensive, experimental study has been conducted at Manchester University on the performance of joints between steel beams and CFT columns, in simple construction, under fire conditions. While there have been extensive studies dedicated to CFT columns themselves, very few have focused on the joint region. This paper suggests that by properly designing and protecting the joints, catenary action can be developed and the steel beam can survive very high temperatures. There are also suggestions pertaining to ideal types of connection components, along with possible design criteria.

Fire Resistant Design of Concrete Filled Tubular Steel Columns
Y.C. Wang and A.H. Orton

The increasing popularity of concrete filled tubular (CFT) columns has made them attractive features in numerous projects. Recently developed design software (Firesoft) makes the design of CFT columns more accessible to structural engineers. This paper offers background information on the design method implemented by Firesoft. Comparisons are brought up with the Eurocode 4 and the modifications the program has made to take into account strength and stiffness degradation of steel and concrete at high temperatures. A study was done to compare the Firesoft calculations against the results of a large number of fire-resistant tests on unprotected and externally protected CFT columns under axial compression or combined axial compression and bending moments. Another study was conducted to propose an interim design method for externally protected CFT columns that use intumescent coating until reliable thermal properties are available on intumescent coating and their applications with CFT columns.

From the November 2008 (Volume 86, No. 21) issue of *The Structural Engineer*, published by the Institution of Structural Engineers.

Simplified Expression for Compression and Bending
Mike Banfi

This paper shows that considering the combined effects of compression and bending in accordance with Eurocode 3 can be complicated. The axial compressive load will further act on the deflected shape, due to the bending moment, and magnify its original moment. This will result in a generally concave interaction curve between compression and bending. The main simplification occurs when the concave interaction curve is shown as a linear interaction, where the linear interaction is taken at the lower bound of the curve. While this method is somewhat conservative, it can be helpful in the initial design phase.

Numerical Validation of Simplified Theories for Design Rules of Transversely Stiffened Plate Girders
Francesco Presta, Chris R. Hendy and Emilio Turco

The behavior of transversely stiffened web panels has been observed and investigated by many, which has caused several theories to emerge. At first the paper compares the different theories and which standards (UK steel code and Eurocode) incorporated the work of which authors (Rockey and Höglund). The remainder of the paper focuses on a nonlinear finite element analysis of stiffeners. There are also comparisons made between the two codes, their validity and what the respected authors have to say about them.

ERRATA

Geometric Formulas for Gusset Plate Design

Paper by JANICE J. CHAMBERS and TONY C. BARTLEY
(3rd Quarter, 2007)

Revise Equation 13 on page 258 as follows:

$$L_2 = \frac{w}{\cos\theta_B} - c\tan\theta_B - L_{Le} \qquad (13)$$

GUIDE FOR AUTHORS

SCOPE: The ENGINEERING JOURNAL is dedicated to the improvement and advancement of steel construction. Its pages are open to all who wish to report on new developments or techniques in steel design, research, the design and/or construction of new projects, steel fabrication methods, or new products of significance to the uses of steel in construction. Only original papers should be submitted.

GENERAL: Papers intended for publication must be submitted by mail to the Editor, Cynthia J. Duncan, ENGINEERING JOURNAL, AMERICAN INSTITUTE OF STEEL CONSTRUCTION, One East Wacker Drive, Suite 700, Chicago, IL, 60601-1802.

The articles published in the *Engineering Journal* undergo peer review before publication for (1) originality of contribution; (2) technical value to the steel construction community; (3) proper credit to others working in the same area; (4) prior publication of the material; and (5) justification of the conclusion based on the report.

All papers within the scope outlined above will be reviewed by engineers selected from among AISC, industry, design firms, and universities. The standard review process includes outside review by an average of three reviewers, who are experts in their respective technical area, and volunteers in the program. The maximum number of papers sent to a single reviewer is three per year, with a frequency of not more than one per quarter. Papers not accepted will be returned to the author. Published papers become the property of the American Institute of Steel Construction, Inc. and are protected by appropriate copyrights. No proofs will be sent to authors. Each author receives three copies of the issue in which his contribution appears.

MANUSCRIPT PREPARATION: Manuscripts must be provided on PC-formatted media, such as a CD-ROM, in Microsoft Word format. A laser-quality proof must accompany your submittal. Fonts and spacing must be suitable for easy reading and reproduction (for the peer-review process). Do not embed photographs, diagrams, illustrations, charts or graphs within the electronic manuscript files. Only equations may be embedded within the flow of the text. Specific requirements for electronic graphics are outlined below. *Engineering Journal* reserves the right not to publish a submittal if suitable graphics cannot be provided by the author.

Title and By-Line: Exact name, title and affiliation of the author or authors are required to appear on the first page of the manuscript.

Body Text: Please restrict font usage to Times, Helvetica, Times New Roman, Arial, and Symbol (for Greek and mathematical characters.)

Headings: All headings should be typed flush left, using upper and lower case, with two line spaces above.

Tables: Each table should appear on its own page. Footnotes to tables should appear below the table, identified by superscripted lower case letters (a, b, c, etc.).

Equations: Whenever possible, equations should be set using Microsoft Equation Editor or MathType (www.mathtype.com). Please set equations using Times New Roman, Times, and/or Symbol fonts.

Captions: Captions should be typed, double-spaced, and located at the end of the electronic manuscript. All photos and graphics must be clearly marked to indicate their corresponding caption.

References: Should be noted clearly in the text and listed, double-spaced, on a separate page in the following sample format.

In text: (Doe, 1992)

In Reference List:

Doe, J.H. (1992), "Structural Steel," *Engineering Journal*, AISC, Vol. 100, No. 1, 1st Quarter, pp. 2–10.

Footnotes: Footnotes should be noted clearly in the text with a superscript asterisk, and should appear at the bottom of the text page, in the following style:

*For a detailed discussion, see...

Graphics (other than photographs): Provide a clear $8\frac{1}{2}$ in. × 11 in. laser-quality proof of each graphic element. Graphics should reproduce cleanly in black-and-white format. Graphics may be submitted and reproduced in color at the Editor's discretion. Please restrict font usage to Helvetica, Arial or Symbol, in sizes suitable for at least 50% reduction (12 pt. minimum). Line weights must be suitable for 50% reduction. When possible, provide each graphic element in a separate electronic file. TIF or EPS file formats are preferred, with a minimum resolution of 300 dots per inch.

Photographs: Provide either original photographs or high-quality electronic files and laser-quality proofs. Electronic photographs may be submitted as grayscale TIF or JPG images, one photograph per file. Photographs may be submitted and reproduced in color at the Editor's discretion. Minimum image resolution is 300 dots per inch. Photographs should be a minimum of 4 in. wide, so the minimum image width is 1200 pixels. Detailed photographs may require resolutions up to 1200 dots per inch. Photos embedded in word-processing documents are not acceptable.

There's always a solution in steel.

ENGINEERING JOURNAL
American Institute of Steel Construction
One East Wacker Drive, Suite 700
Chicago, IL 60601